FINAL TECHNICAL REPORT

HIGH-RESOLUTION GEOPHYSICAL AND GEOLOGICAL INVESTIGATIONS OF LOWER WABASH VALLEY FAULT SYSTEM NEOTECTONICS

Award Number: 05HQGR0091

Principal Investigator: Edward W. Woolery
University of Kentucky
Department of Earth and Environmental Sciences/
Kentucky Geological Survey
101 Slone Research Building
Lexington, KY 40506-0053
Phone: 859.257.3016
Fax: 859.323.1938
Email: woolery@uky.edu
http://www.uky.edu/AS/Geology/

Co-Investigator: James Whitt
University of Kentucky
Dept. of Earth and Environmental Sciences
Lexington, KY 40506-0053
jameswhitt@hotmail.com

Co-Investigator: Roy B. VanArsdale
University of Memphis
Department of Earth Sciences
Memphis, TN 38152-3430
Email: rvanrsdl@memphis.edu
Phone: 901.678.4356

Program Element: CU/I

Key Words: Neotectonics, Quaternary Fault Behavior, Reflection Seismology

Award Number: 05HQGR0091

HIGH-RESOLUTION GEOPHYSICAL AND GEOLOGICAL INVESTIGATIONS OF LOWER WABASH VALLEY FAULT SYSTEM NEOTECTONICS

Edward W. Woolery, *Dept. of Earth & Environmental Sciences, University of Kentucky, 101 Slone Bldg., Lexington, Ky. 40506, Tel: 859.257.3016, Email: woolery@uky.edu*,

ABSTRACT

Seismic reflection (P- and SH-wave), correlative drilling, and age dating data provide evidence of neotectonic deformation along the Caborn (CF) and Hovey Lake (HLF) faults, in the Wabash Valley fault system (WVFS). The WVFS is a series of high-angle normal faults located primarily in southern Indiana and Illinois. Since their formation, these faults have likely been transpressionally reactivated in the contemporary E-W-oriented compressive stress state. Second-order paleoliquefaction evidence show the WVFS has experienced large prehistoric earthquakes, but only moderate magnitude historic and contemporary events; therefore, the seismic potential in this region is poorly defined.

The bedrock expressions of the CF and HLF were imaged with seismic reflection data (P-wave). Higher resolution analyses were performed with SH-wave seismic imaging was used to characterize structure that extended into the overlying Quaternary sediments. Anomalous features were cored to verify structure, and to collect datable material. The CF and HLF are interpreted to extend into the uppermost five meters of sediment and to displace horizons dated to 19,740 and 31,000 years before present, respectively. Displacement along the HLF is interpreted to extend 2-3 meters above the associated age date. These structures represent late Quaternary primary coseismic deformation in the WVFS.

NONTECHNICAL SUMMARY

Subsurface geophysical images and correlative drilling within the southern Wabash Valley have provided evidence for tectonic activity during the Quaternary. The images, along with carbon-14 age measurements derived from organic samples collected from our drilling activities, have enabled us to approximate the time of movement and understand the style and geometry of the deformation. The resolution limits of our geophysical imaging suggests that deformation anomalies are within 6 meters of the ground surface; reliable age results from subsequent core samples suggest deformation as late as 19.7 ka. There are limitations to the resolving power of each geophysical and geological exploration technique used; consequently, the exact timing of the latest tectonic episode remains unknown. We hope to coordinate and provide target information to researchers specializing in paleoseismologic trenching in order to reduce the uncertainty. Our results have design implications for high-hazard and critical facilities in the area. In addition, the findings also contribute to the USGS-NEHRP central U.S. efforts to locate/ characterize seismogenic faults in order to better constrain seismic source zone boundaries.

1. Introduction

1.1. Problem

This study assessed the extent, as well as the physical and temporal characteristics of the neotectonic deformation in the southernmost part of the Wabash Valley Fault System (WVFS), near the northern New Madrid seismic zone (NMSZ) boundary suggested by Wheeler [1997] (Figure 1.1). Accurate identification and characterization of near-surface geologic structures in the expansive river valleys of the seismically active central United States is often impeded by relatively thick sequences of unlithified sediment [Woolery, 2005]. The soft sediment cover conceals neotectonic bedrock structure and, apart from a few notable exceptions (i.e., Crowley's Ridge, Reelfoot Scarp, Commerce Fault, and possibly Sikeston Ridge), the sediment's inherently weak mechanical and erodable properties commonly fail to transform near-surface propogated faults and folds into significant or noticeable surface geomorphic features [Woolery, 2005]. Although Bear et al. [1997] reported that the Quaternary sediment overlying the WVFS exhibits no neotectonic surface expressions; recent studies (e.g., Woolery et al., 2004; Rutledge, 2004; Woolery, 2005) have found that these observations do not preclude Quaternary fault activity, because these surfaces are active flood plains.

The study focused on the northern Hovey Lake (HLF) and Caborn (CF) faults (Figure 1.2). These structures are within the error ellipse of several historical earthquakes, and the CF is approximately coincident with the epicenter of the moderate-sized ($m_{b,Lg}$ 5.0) 18 June 2002 earthquake (Figure 1.3). This work is a continuation of research that has thus far found evidence of neotectonic deformation extending ~4 meters (m) above a Quaternary horizon, C^{14} dated to ~32,000 years before present (YBP), along the southernmost Hovey Lake fault. The more recent deformation may provide first-order paleoseismological evidence for the large earthquakes suggested from the widely distributed paleoliquefaction features in the area [Obermeier et al., 1993; Munson et al., 1995; Munson et al., 1997; Pond and Martin, 1997].

1.2. Objectives

This geophysical and geological field investigation integrates high-resolution compression (P-wave) and shear-wave (SH mode) seismic reflection profiling, ground-penetrating radar, and correlative drilling. This investigation further assesses the extent, timing, and geometry of Quaternary-aged deformation in the unlithified sediment overlying the northern HLF and CF of the WVFS (Figure 1.2). It is complementary to other research projects that aimed to locate and characterize potential source structure beyond the northern Mississippi embayment [e.g., McBride et al., 2002, 2003; Woolery et al., 2002, 2003, 2005]. High-resolution P-wave and SH-wave seismic reflection techniques were used to locate the faults. SH-wave (shorter spatial interval) and ground-penetrating radar profiling were used to image near surface expressions of these faults. Areas with structure extending into the late-Quaternary section were cored and sampled for seismic correlation and Carbon-14 age determination.

1.3. Scientific and Engineering Significance

Evidence for the CF and HLF extending into the Quaternary sediments suggests first-order neotectonic deformation has occurred above reactivated Paleozoic structures. Furthermore, such evidence would suggest that there is not a discontinuity between seismogenic basement faults and those found in the near surface.

Identifying discrete seismogenic structures and source zone boundaries improves seismic hazard assessment. As ground-motion modeling techniques and the associated databases of dynamic crustal properties continue to improve, definition of potential seismogenic sources in the central United States remains poorly characterized. Delineation of seismogenic geologic structure based on instrumentally derived hypocentral locations/trends is currently problematic, because of the modest rate of seismicity and inadequate seismic network coverage in the larger area. Consequently, existing seismic hazard estimates for prescribed design-level earthquakes in the region are primarily based on “floating”-events. Depending on the assigned boundary conditions associated with this approach, calculated site-specific ground motions can possess considerable uncertainty.

Paleoseismological evidence, historical earthquake accounts, and contemporary earthquake records indicate that the lower Wabash Valley of southern Illinois and Indiana has a significant seismic hazard. The pre-instrumental and instrumental evidence of seismicity also indicate that small to moderate earthquakes have occurred in an area roughly coincident with existing geologic structure (Figure 1.3). The low rate of seismicity (relative to the NMSZ) and insufficient network coverage (outside the most active part of the NMSZ) make integrated field investigations of potential seismogenic geological structure the most efficient and cost-effective method of assessing such areas.

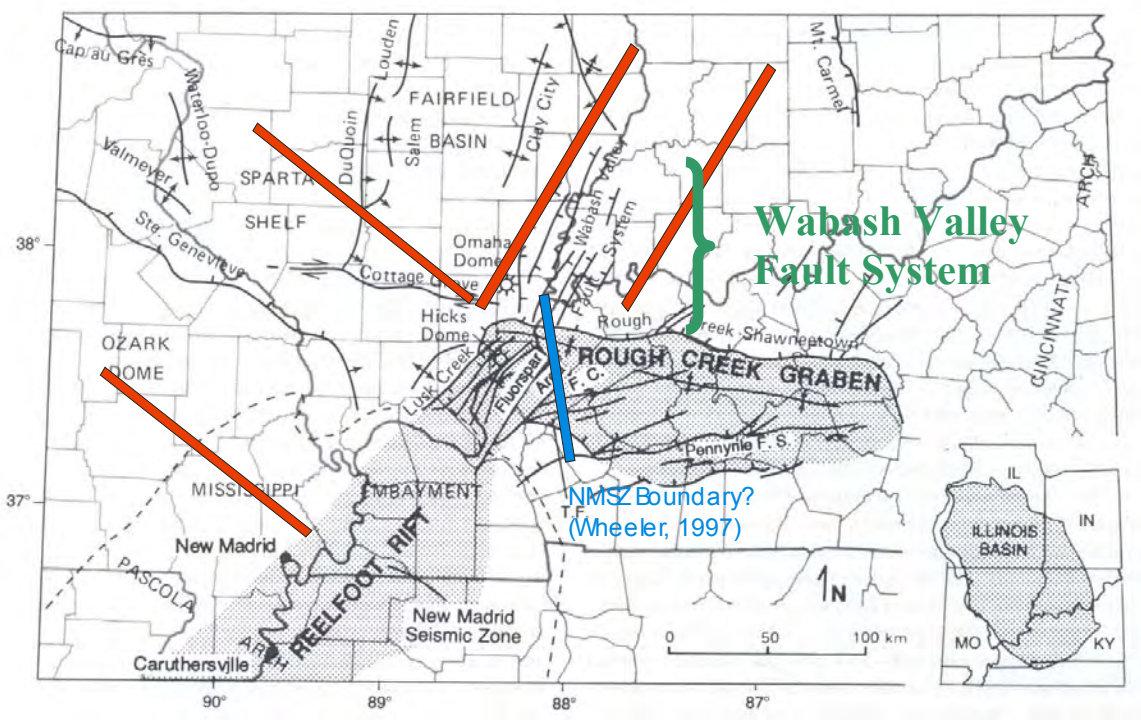

Figure 1.1 Regional structural features in the central U.S. (modified from Kolata and Hildenbrand, 1997) and inferred quadruple junction (red lines) from Braile et al. [1986]. The blue line represents the NMSZ boundary that was suggested by Wheeler [1997].

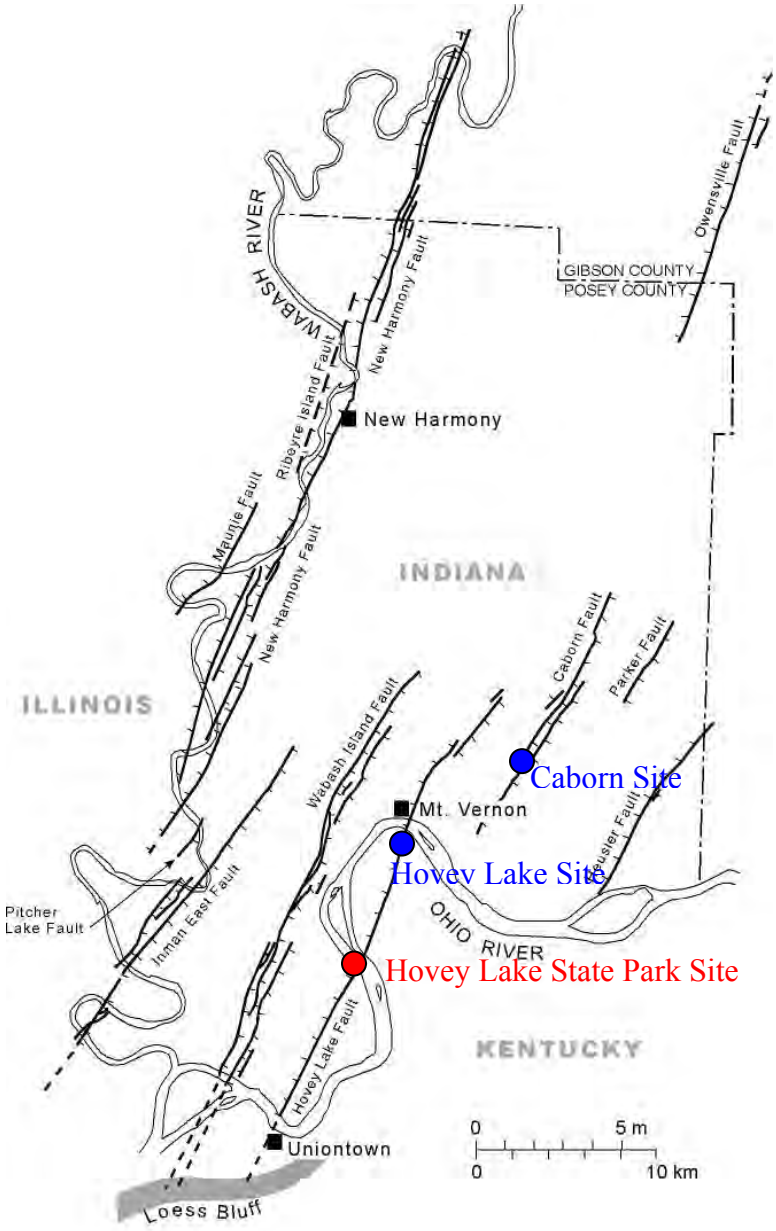

Figure 1.2 Location of major faults in the lower WVFS and their relationship to existing HLF and newly acquired HLF/CF geophysical profiles (modified from Woolery, 2005).

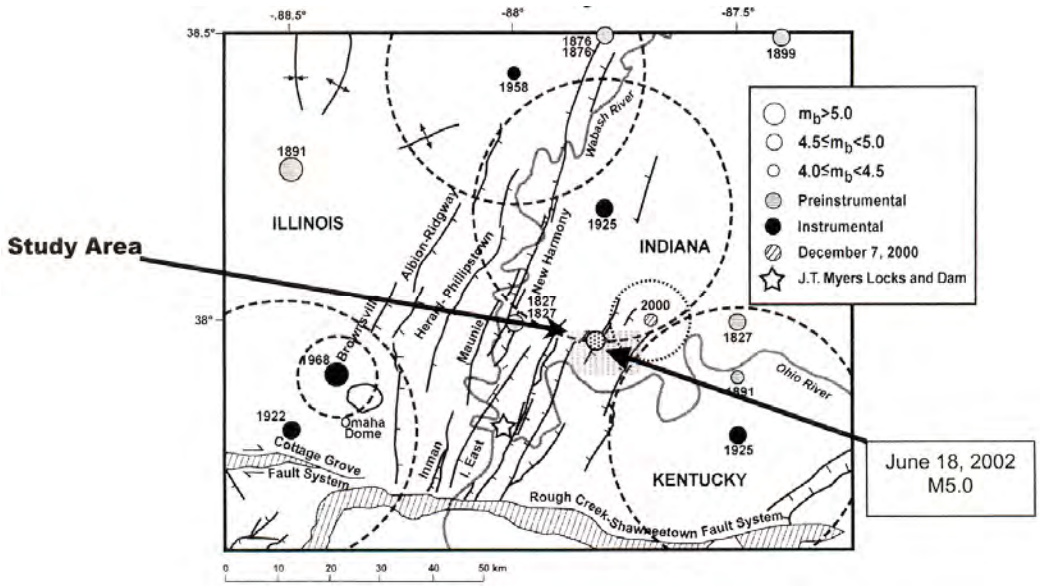

Figure 1.3 Location of historical and contemporary earthquakes in relationship to WVFS (modified from Bear et al., 1997 and Street et al., 2002). The arrows point out the study area that contains the Caborn fault and the location of the June 18, 2002 earthquake. The dashed circles indicate epicentral uncertainty.

2. The Wabash Valley Fault System

2.1. Background and Conceptual Framework

2.1.1. Geologic and Tectonic History

Heigold and Kolata [1993] suggested a crustal boundary exists at the southern end of the Illinois Basin, based on seismic reflection data. They stated the boundary is characterized by a WNW-trending Proterozoic terrane boundary that is approximately 40 km wide and believed to have formed prior to 1.48 Ga (+/- 30 m.y.). Their boundary is located along the projected trend of the Central Plains orogen, which ranges in age from 1.63 to 1.80 Ga. On the north side of the boundary, there is a sequence of layered Proterozoic rocks up to 11 km thick and high magnetic intensity values; on the south side, there is a lack of basement reflectors and low magnetic intensity values [Heigold and Kolata, 1993]. They suggested the boundary separates the WVFS from the NMSZ, because the regions appear to have different basement structure. The location of the boundary coincides with the south-central magnetic lineament (SCML), which is a continental-scale crustal discontinuity that may be the result of a late Precambrian shear zone [Hildenbrand and Ravat, 1997]. The SCML is characterized by a steep magnetic gradient immediately south of a series of closed magnetic highs [Heigold and Kolata, 1993]. Many igneous intrusions are located in the shallow and deep crust in this area.

Formation of the Reelfoot Rift and Rough Creek Graben is an important part of the regional tectonic history because it influenced the formation of the WVFS (Figure 2.1) [Heigold and Kolata, 1993]. The formation took place in Late Precambrian or Early Cambrian time due the breakup of the supercontinent Rodinia. The supercontinent breakup formed several aulocogens and strike-slip faults [Hildenbrand et al., 1996]. The proto-Illinois basin began as one of these failed rifts [Kolata and Nelson, 1991].

The Greyville graben also formed during rifting (late Proterozoic-early Paleozoic) and may result from stress generated by a bend in the Reelfoot-Rough Creek-Rome rift system [Hildenbrand and Ravat, 1997]. The Greyville graben lies beneath and likely influenced the formation of the WVFS. Thomas [1993] stated that the bend may have formed where the Reelfoot Rift met an oblique transfer zone that created the Rough

Creek Graben. Furthermore, a dislocation stress is created by bends in shear or tensile cracks and may lead to secondary faulting [Hildenbrand and Ravat, 1997].

Kolata and Nelson [1991] indicated that faulting within the rift complex came to a halt in Late Cambrian time, and the tectonic setting slowly changed from a rift basin to a broad, slowly subsiding cratonic embayment. They also concluded regional downwarping occurred throughout most of the Paleozoic and formed a broad southward-plunging trough, which characterized the proto-Illinois basin. During this time period the basin was open to marine circulation and subsided faster than the surrounding areas [Kolata and Nelson, 1991]. Due to the rise of the Kankakee arch, the Illinois basin area was separated from the Michigan basin in Ordovician time, and the area continued to subside more than the surrounding arches throughout the Paleozoic [Kolata and Nelson, 1991].

In the case of the WVFS, the bend in the rift system likely concentrated stress throughout the Phanerozoic, which is supported by deformation and intrusive events in the Devonian, Mississippian, Pennsylvanian, and Permian [Hildenbrand and Ravat, 1997]. The Cottage Grove Fault System and Ste. Genevieve Fault Zone are shown, to the west of the WVFS, in Figure 1.1 and are thought to have formed in a similar manner.

Rene and Stanonis [1995] did not find evidence of rift-fill immediately above Precambrian basement, in their seismic reflection imaging of the Wabash Island and Hovey Lake faults. This led to their conclusion that these basement faults were not reactivated. Nelson [1990b] interpreted seismic data to show that faults in the Paleozoic layers lose displacement with depth and do not continue below 4 km depth. Another proposal by Nelson [1991], suggested that NW-SE compressive stresses related to continental collision in the late Paleozoic arched the region and formed the WVFS.

The Reelfoot Rift and Rough Creek Graben form a continuous rift system, which has been reactivated episodically during the Phanerozoic, and control the formation of surficial faults [Heigold and Kolata, 1993]. This rift system has also influenced seismicity and formation of the Illinois basin. Because the rift system is the major

structural feature in the region, its evolution influences the formation of the surrounding minor structures. Thick sections of sediment were deposited as the Reelfoot basin periodically subsided from the early Paleozoic to the Middle Pennsylvanian [Hildenbrand et al., 1996]. As the rift system began to subside, the Rough Creek-Shawneetown Fault System and Lusk Creek Fault Zone formed along its margins (Figure 1.1) [Heigold and Kolata, 1993]. The related faults have surficial expressions that resulted from reactivation related to both compression and extension, which took place during the late Paleozoic and early Mesozoic [Heigold and Kolata, 1993]. Compression resulted from continental collision, and reactivated the boundary faults of the Reelfoot rift and Rough Creek graben in Late Pennsylvanian and Early Permian time [Kolata and Nelson, 1991].

The Cottage Grove Fault System likely formed during the early Permian; at this time, the regional stress field caused right-lateral wrenching, which is believed to have induced horizontal slip along a basement weakness [Heigold and Kolata, 1993]. Hildenbrand and Ravat [1997] suggested this basement weakness might coincide with the Proterozoic terrane boundary. They also suggested the fault system served as a pathway for magma that formed some intrusions related to the SCML. These igneous intrusions formed the Tolu arch and Hicks Dome (Figure 1.1) around this same time [Heigold and Kolata, 1993]. Hicks Dome and associated diatremes are locations where igneous pressures were violently released [Kolata and Nelson, 1991]. The Tolu arch, which was located along the southwest margin of Hicks Dome, collapsed as magma migrated away; a remnant of this pluton is represented by a magnetic anomaly centered ~10 km northeast of Hicks Dome [Kolata and Nelson, 1991].

Hildenbrand et al. [1996] proposed the presence of two shallow intrusions in the southern Illinois Basin, in or near the WVFS, which were emplaced in the late Paleozoic. Based on the correspondence of dikes and mapped faults, Hildenbrand and Ravat [1997] concluded the Wabash Valley faults acted as pathways for ascending magma. They also found that the dikes have a similar age to the faulting. The abundance of dikes detected suggested to them that more faults exist than what have been mapped in the WVFS. In the late Paleozoic, magmas were injected into the Wabash Valley faults, which may have

formed as tension fractures from the rise and collapse of a dome [Hildenbrand and Ravat, 1997]. They suggested this magma ascended along preexisting basement faults that were created during Precambrian-early Paleozoic rifting and may include the margins of the Greyville Graben. The age and composition of the Wabash Valley dikes is also similar to those in the Cottage Grove Fault System (Figure 1.1).

Uplift occurred in the late Paleozoic and Mesozoic, forming the Pascola Arch (Figure 1.1) and the southern margin of the Illinois Basin [Hildenbrand et al., 1996]. This uplift occurred during an extensional phase that began after Early Permian time [Kolata and Nelson, 1991]. The extensional faulting occurred along the Reelfoot rift and Rough Creek graben during the breakup of Pangea, and the northwest-southeast tension began and caused normal faulting throughout a region that likely included the WVFS. The Pascola Arch was subsequently buried beneath the Mississippi Embayment as the lower crust cooled and isostatically adjusted [Kolata and Nelson, 1991].

Large plutonic bodies were emplaced along the margins of the Reelfoot graben, in the Cretaceous or later [Hildenbrand et al., 1996]. Subsidence and deposition began again in the Late Cretaceous, leading to very thick (~1 km west of Memphis, TN) sections of sediment in and around the Mississippi Embayment [Hildenbrand et al., 1996]. In the recent geologic past, the stress state in the region of the WVFS has been nearly east-west compression. The change has occurred within the last 70 million years, as North America has drifted westward, away from the Mid-Atlantic ridge [Kolata and Nelson, 1991]. As a result, many faults in this region have been reactivated in a reverse and/or strike-slip nature (i.e., transpressional motion).

2.1.2. Structure of the WVFS

The WVFS is a linear north-northeast trending series of high angle normal faults, which form a band of narrow graben structures, that are roughly coincident with the Wabash River valley of southern Indiana and Illinois (Figure 1.2) [Woolery, 2005]. The normal faults formed in an extensional regime, which is much different from the current stress state. The largest faults in this system bound the 22-km wide, 40-km long Grayville

Graben [Bear et al., 1997]. These faults were first recognized during petroleum exploration in the early twentieth century [Bear et al., 1997]. Since then, continued drilling and deep geophysical imaging have determined that the faults are rooted in a series of basement-penetrating faults at seismogenic depths [Rene and Stanonis, 1995]. Conversely, industry lines have been interpreted to show that the Paleozoic faults do not penetrate basement rocks in the western portion of the WVFS [McBride et al., 1997]. The Inman East fault lies 7-12 km to the west of the HLF, and the faults west of the Inman East fault are the ones that may not penetrate basement rocks. The HLF dips down to the west and forms the eastern margin of the Mt. Vernon graben. The other margin of this graben is formed by the Wabash Island fault. The CF is located 3-5 km east of the HLF and dips down to the east (Figure 1.2).

2.1.3. Relationship of WVFS to Regional Structure

There is a lack of scientific consensus regarding the complex seismotectonic relationship of the WVFS to other major regional geologic structures (i.e., Fluorspar Area Fault Complex, Rough Creek Fault Zone, Reelfoot Rift, etc.). A map showing the significant structural features and current stress state of the Midcontinent can be seen in Figure 2.1. Braile et al. [1982, 1986, 1997] describe a rift complex (quadruple junction) that includes the Reelfoot Rift, Rough Creek Graben, and two additional arms called the St. Louis Arm and the Southern Indiana Arm (includes the WVFS). This rift complex, which was named the New Madrid rift complex, was proposed as a result of studies using gravity, magnetic, and seismic data [Braile et al., 1982, 1986]. Sexton and others [1986] interpreted the Greyville graben as part of the Southern Indiana arm of the proposed quadruple junction. Greb [1989] proposed that the Southern Indiana arm might roughly coincide with the WVFS and its NNE trend.

Conversely, other researchers question the geological continuity of the structures. The differing interpretations are based on deep seismic-reflection data, as well as, the lack of prominent potential field anomalies extending from the central Reelfoot Rift into southern Illinois and Indiana [Bear et al., 1997; Hildenbrand and Ravat, 1997]. In addition, the presence and structure of the SCML [Hildenbrand, 1985; Heigold and

Kolata, 1993] adds to the enigma. There is a difference in crustal composition and structure across the SCML [Heigold and Kolata, 1993]. Furthermore, the characteristics of the more localized Paducah gravity lineament (PGL) do not support the proposed St. Louis Arm, despite the two having a coincident location [Hildenbrand et al., 1996]. The PGL is much shorter in length than the Reelfoot rift and Rough Creek graben [Hildenbrand et al., 1996]. There is also a lack of data for the existence of an associated graben or rift-related sedimentary rocks along the PGL [Kolata and Nelson, 1991].

Bear et al. [1997] suggested significant fault offsets are restricted to a zone between 38.35ºN and 38ºN and that the Greyville graben is not a NE extension of the structural complex composed of the Rough Creek Fault System and the Reelfoot Rift. In this zone, seismic reflection data showed that structural trends are laterally offset across several large faults, indicating strike-slip motions of 2 to 4 km [Bear et al., 1997]. Based on correlation of major faults with steep potential field gradients, they also suggested fault positions are controlled by major lithologic contacts within the basement and faults may extend into the depth range where earthquakes are generated.

Numerous NW- to NNE-trending ultramafic dikes and six intrusive complexes have been resolved by enhanced short-wavelength magnetic anomalies [Hildenbrand & Ravat, 1997]. Some of the dikes follow mapped faults and their abundance may signify the presence of unknown faults [Hildenbrand & Ravat, 1997]. The interpreted dikes and mapped faults terminate near the Reelfoot-Rough Creek-Rome rift system [Hildenbrand & Ravat, 1997]. Interpretation of regional gravity and magnetic data suggested to Hildenbrand & Ravat [1997] that the shallow faults and deep-seated rift structures in the Wabash Valley terminate at or near the Rough Creek-Shawneetown Fault System. Furthermore, the proposed Indiana arm is considerably wider than the Greyville Graben and the margins of the mapped WVFS [Hildenbrand and Ravat, 1997]. If the WVFS made up the Southern Indiana arm, then the margins of the arm should coincide with fault locations, as is the case with the Reelfoot Rift and Rough Creek Graben. The Greyville graben is considerably smaller in cross section than the Reelfoot Rift and Rough Creek Graben. When compared to the Reelfoot Rift and Rough Creek Graben, Wabash Valley

faults are minor tectonic structures and probably do not represent a failed rift arm [Hildenbrand & Ravat, 1997]. Nelson and Lumm [1984] found similar results in their study of drill-hole data and exposures in underground coalmines. Previous studies, by Hildenbrand et al. [1982] and Hildenbrand and Hendricks [1995], also concurred that the proposed St. Louis rift arm is a local feature related to stress accumulations at the bend, and not part of a rift system.

2.1.4. Seismicity

The WVFS has experienced large earthquakes in prehistoric times [Obermeier et al., 1993]. Clastic dikes, interpreted as liquefaction features, from southern Indiana and Illinois suggest that at least eight earthquakes strong enough to cause widespread liquefaction ($M_w \geq 6$) have occurred in the past 20,000 years [Munson et al., 1997]. Three of these earthquakes took place within 25 km of the WVFS [Hildebrand & Ravat, 1997]. At least two prehistoric events from this region have been estimated to exceed **M**7, and the strongest prehistoric earthquakes coincide with the zone of greatest historic seismicity [Munson et al., 1997]. Pond & Martin [1997] estimated magnitudes for four prehistoric earthquakes in the Wabash Valley. Their geotechnical and seismological investigation estimated surface accelerations likely for **M**7.8, **M**7.3, **M**7.1, and **M**6.9 events [Pond & Martin, 1997]. These estimates correspond to the Vincennes, Skelton, Vallonia, and Waverly earthquakes respectively [Pond & Martin, 1997].

Street et al. [2004] suggested that the moment magnitudes for these four prehistoric earthquakes should be 0.6-0.8 units less than the Pond and Martin [1997] estimates. These changes are attributed to scaling down the magnitude of the 31 October 1895 earthquake (from 6.8 to a range of 5.9-6.2) and recalibrating the curve used for magnitude estimates (moment magnitude vs. maximum distance to surface evidence of liquefaction) [Street et al., 2004]. These researchers also determined from the 1 March 1925 and 18 June 2002 earthquakes that liquefaction can occur at greater distances from the source and from smaller magnitude events, respectively, than suggested by Pond and Martin [1997]. Olson et al. [2005] recalculated magnitudes for these events based on their reassessment of maximum distances to liquefaction features and liquefaction

susceptibility. In their recalculations, they used accepted magnitudes and site to source distances, which were measured in a consistent manner, for relevant historic earthquakes [Olson et al., 2005]. Their results were equivalent to the magnitudes proposed by Street et al. [2004].

The Vincennes earthquake occurred near Vincennes, Indiana between 5,900 and 6,300 YBP [Munson et al., 1995]. This earthquake has been estimated as a M ~7.5 or greater and to have caused extensive liquefaction and large dikes, with sandblows, in an area from 95 km north-northeast to 85 km south-southwest of Vincennes [Munson et al., 1995]. Obermeier et al. [1995] suggest this earthquake produced sand blows in an area spanning at least 175 km from north to south and 105 km from east to west. The dikes range in width from a few centimeters to as much as 2.5 meters [Obermeier et al., 1993]. Formation of these dikes requires severe ground shaking, which is much greater than any earthquake has caused in the central United States since the 1811-12 New Madrid earthquakes [Obermeier et al., 1993]. Although the span of liquefaction features for the Vincennes earthquake is less than that of the largest New Madrid quake, it is much more than the 1895 Charleston, Mo. earthquake and similar to the 1886 Charleston, S.C. quake [Obermeier et al., 1993].

An earthquake approximately 12,000 YBP (+/- 1000 yr) was interpreted with an estimated 7.1-7.3 magnitude [Munson et al., 1997]. They refer to this event as the Skelton-Mt.Caramel earthquake due to its proximity to the corresponding cities in Indiana and Illinois, respectively. The epicenter of this event is approximately 40 km southwest of Vincennes, IN; liquefaction features have been observed in Indiana about 50 to 60 km north, east, and south of the epicentral area. These features also lie within the zone that encompasses liquefaction features from the Vincennes-Bridgeport earthquake [Munson et al., 1997].

The Vallonia earthquake was located about 100 km east of the Wabash River, in the East Fork valley, and occurred 3,950 YBP (+/- 250 yr) [Munson et al., 1997]. They estimated a moment magnitude of 6.9-7.1. An earthquake of similar magnitude, the Martinsville-

Waverly event, occurred 30-50 km southwest of Indianapolis between 8,500 and 3,500 YBP [Munson et al., 1997]. Both events took place in areas of very low and infrequent historic seismicity [Munson et al., 1997].

Evidence exists for two other prehistoric earthquakes in Indiana [Munson et al., 1997]. The magnitude estimates for both are approximately six [Munson et al., 1997]. One event occurred 4000 YBP (+/- 500 yr) ~35 km southeast of Vincennes, and the other 2000 YBP (+/- 500 yr) ~60 km east-northeast of Vincennes [Munson et al., 1997]. Despite efforts to find liquefaction features, there is little evidence of strong shaking along the Ohio River, in proximity to the WVFS, during the last 4,500 years [Munson et al., 1997]. It is possible that many large prehistoric earthquakes have taken place in areas lacking liquefiable deposits, however [Munson et al., 1997]. For example, it is possible that liquefaction was prevented by areas with too thick of a sedimentary cap or large fluctuations in river level [Munson et al., 1997].

Conversely, prehistoric events greater than **M**6 have occurred outside the WVFS in areas of little or no historic seismicity [Munson et al., 1997]. There is liquefaction evidence to suggest a ~**M**6.9 earthquake in south-central Indiana between 3,700 and 4,200 YBP [Munson et al., 1995]. Hildenbrand & Ravat [1997] stated there is no obvious relation between the Wabash Valley Fault System and the epicenters of historic and prehistoric earthquakes, however.

Historically, the seismicity rate in the WVFS has been significant. Numerous small to moderate magnitude earthquakes have been documented in and around the boundaries of the proposed study area during the past 200 years (Figures 1.3 and 2.2). The largest earthquake proximal to the WVFS since regional seismic networks were established was the 9 November 1968 magnitude 5.5 ($m_{b,Lg}$) that was located along the fault system's southwestern boundary [Woolery, 2005]. This event is thought to be the result of blind thrust faulting in crystalline basement [McBride et al., 1997]. This is also the largest earthquake in the central U.S. during the 20th century [Bear et al, 1997]. This earthquake,

as well as 17 other damaging earthquakes (Modified Mercalli VI or greater), is shown in Figure 2.2 [FMSM Engineers, 2002].

Earthquake focal mechanism studies in the WVFS show that the primary type of slip is right-lateral strike-slip (Figure 2.3) [Taylor et al., 1989; Kim, 2003]. On June 10, 1987 there was an earthquake, 4.9 m_b, in the northern limit of the WVFS (Figure 2.2 and 2.3) [Kim, 2003]. Its focal depth was approximately 10 km, with numerous aftershocks at depths ranging between 10 and12 km [Kim, 2003]. The March 6, 2000 event (2.7 m_b) just north of Evansville, IN had a focal depth of 5 km, and the December 7, 2000 earthquake (3.9 m_b) was within approximately 5 km of the HLF's northern end [Woolery et al., 2004]. The focal depth for the latter event was ~5 km. Inside the WVFS, earthquakes at depths such as these are likely related to faults belonging to the WVFS, rather than disconnected basement structure [Woolery et al., 2004].

More recently, there was a magnitude 5.0 (m_b) earthquake on 18 June 2002 (Figure 2.2 and 2.3), and its epicenter was near the CF [Kim, 2003]. The strike and dip of a nodal plane from the source mechanism coincides with the trend and dip angle of the CF [Kim, 2003]. At least one aftershock that had a similar location, depth, and focal mechanism was recorded as well [Won-Young Kim, 2006, Personal Communication]. Therefore, this event may be related to the CF. Kim [2003] estimated the focal depth to be between 16 and 20 km. The source mechanism for this event is predominantly strike-slip along near-vertical nodal planes [Kim, 2003]. This earthquake is likely the result of reactivation of buried, high-angle faults, associated with Precambrian rifting, by the present east-west-trending regional horizontal compressive stress [Kim, 2003]. Five more earthquakes with **M**5.0-5.5 have been documented within the WVFS in the last 200 years [Munson et al., 1995].

Coal mines within the WVFS, have exhibited thrust faults that have displaced Mississippian and Pennsylvanian strata by a few inches to a few feet; moreover, many of the faults are thought to be tectonic in origin [Nelson and Lumm, 1984; Ault et al., 1985; Nelson and Bauer, 1987]. The faults strike approximately north-south and dip less than

45° east or west. This is additional evidence for transpressional reactivation of the WVFS in the current mid-continent stress state [Woolery et al., 2004]. A broad anticline in the uppermost 4 km of the Mt. Vernon graben may also be evidence of transpressional strain [Woolery et al., 2004]. Conversely, Rene and Stanonis [1995] attributed the presence of this anticline to reverse-drag folding that resulted from the extensional formation of the Mt. Vernon graben.

Although the Midcontinent Stress Province could be responsible for reactivation in the WVFS, the Commerce geophysical lineament (Figure 2.1) provides another possible explanation for the current seismicity. The CGL runs through the northern edge of the WVFS, and Holocene displacement has been observed on the coincident faults [Harrison et al., 1999]. Hildenbrand and Ravat [1997] suggested at least five large prehistoric earthquakes occurred near the surface projection of the CGL. McBride et al. [1997] also stated that basement reflectors of the CGL coincide with the hypocenter of the November 9, 1968 earthquake.

2.1.5. Stratigraphy

The deeper stratigraphy in the area of the Mt. Vernon graben is shown in Figure 2.4. The Eau Claire Formation lies on top of the crystalline basement (granite, rhyolite, granodiorite, and basalt) [Kolata and Nelson, 1991]. The Eau Claire Formation is made up of carbonate and siliciclastic rocks of Cambrian age [Kolata and Nelson, 1991]. The Knox Group overlies the Eau Claire and contains carbonates and siliciclastics that are primarily Ordovician in age [Kolata and Nelson, 1991]. The overlying Maquoketa Group is made up of Ordovician siliciclastic sediments that were eroded from the eastern highlands [Kolata and Nelson, 1991]. The New Albany Shale lies on top of the Maquoketa Group and was deposited in the Devonian and early Mississippian [Kolata and Nelson, 1991]. The Ste. Genevieve Limestone overlies the New Albany Shale and is Mississippian in age [Bristol and Treworgy, 1979]. The upper bedrock in the study areas is mostly Pennsylvanian sandstone, shale, coal (with clays), and occasional interbedded carbonates [Woolery, 2005].

Johnson and Norris [1976] reported that as much as 45 m of unlithified Quaternary alluvial and lacustrine sediment overlies the bedrock, and the sediment overburden generally consists of Pleistocene to Holocene clays underlain by a fining-upward sand sequence. Woolery [2005] continuously sampled four boreholes within 3 km of the HLF, within or near (<2 km) the Hovey Lake State Park. Bedrock (shale) was reached at depths between 10 and 34 m [Woolery, 2005]. He also found that the sediment immediately overlying bedrock consisted of ~5 m of well (SW) to poorly (SP) graded sands, and this was overlain by 5.5 m of low-plasticity (CL) silty clays (lacustrine?) [Woolery, 2005]. Two organic samples from one of the boreholes produced carbon-14 ages of 36,980 (+/- 450) YBP and 39,480 (+/- 620) YBP from depths of 7.7 and 9.0 m, respectively [Woolery, 2005].

2.2. Previous Related Work

This study is an outgrowth of results originally attained from a high-resolution shear wave profile collected in association with the design of a Corps of Engineers' 1,200-foot lock chamber, at the J. T. Meyers Locks and Dam, near Uniontown, KY on the Ohio River (immediately upstream of its confluence with the Wabash River) (Figure 1.2) [FMSM Engineers, 2002]. Specifically, the original study examined variation in the top-of-rock elevation across the Wabash Island Fault (WIF) and HLF, because they were situated beneath the proposed lock's downstream and upstream approach walls, respectively. The WIF and HLF were originally recognized by the numerous petroleum boreholes in the area and were subsequently imaged by Rutledge [2004] and Rene and Stanonis [1995].

Rutledge [2004] imaged the Quaternary sediments that overlie the Mt. Vernon graben with 7.5 km of high-resolution SH-wave seismic reflection data. He interpreted 46 faults with varying types and amounts of displacement [Rutledge, 2004]. Carbon-14 (^{14}C) dating of displaced horizons suggested movement between approximately 26,000 and 42,000 YBP [Rutledge, 2004].

Rene and Stanonis [1995] collected deep seismic-reflection profiles in order to study basement structure in the Illinois Basin. They interpreted the WIF as having several branches (including the HLF) in a quasi-planar zone with the primary offset at depth as high-angle, north-northeast to northeast-trending normal displacement [Rene & Stanonis, 1995]. The upper part of the HLF lies 3 km to the east of the upper WIF [Rene & Stanonis, 1995]. The HLF is listric and displacements along it decrease with depth [Rene & Stanonis, 1995]. The WIF and HLF intersect near a depth of 5.5 km and form the boundaries of the Mt. Vernon graben (Figure 2.4) [Rene & Stanonis, 1995]. Below the intersection, the WIF continues into the basement rock [Rene & Stanonis, 1995]. In addition, Rene and Stanonis [1995] suggested the faults disturb the youngest lithified strata (i.e., late Pennsylvanian), but not the overlying Quaternary sediment (i.e., Pleistocene and Holocene). Their upper age boundary (pre-Pleistocene) was based on incoherent (early in the time section), lower resolution seismic data, and thus is not well constrained.

Part of the ongoing National Earthquakes Hazards Reduction Program (NEHRP) work was a high-resolution shear-wave reflection profile conducted, across the southern HLF, to determine if deformation extended above bedrock and into Quaternary sediment. The data were acquired in the Hovey Lake State Park reservation because of easy accessibility (Figure 1.2). Two coincident SH-wave (different spatial intervals) common-depth-point (CDP) profiles were collected (Figure 2.5). A reconnaissance profile was collected in order to isolate the bedrock structure, and the subsequent coincident profile was collected in order to optimize the recording window of the Quaternary sediments. Figure 1.8 is part of the stacked profiles that focused specifically on the HLF. Top-of-bedrock, which is highly disrupted along the profile length, occurs between 10 and 35 m depth. An offset, at the top of bedrock, of approximately 10 m was interpreted and is consistent with estimations by Rene and Stanonis [1995]. An overlying coherent reflector was imaged and corresponds to depths between 5 and 8 m below the ground surface. An offset of approximately 3 m was interpreted between traces 100 and 300. In addition, a subtle upwarped or antiformal structure is exhibited between trace numbers 150 and 300 that may suggest an episode of transpressional movement. Prior drilling and sampling in the

vicinity of the profile found a coarse sand horizon at 9 m (just above bedrock); but more importantly, ^{14}C age dates obtained from organic material in the samples placed the horizon at approximately 32,000 YBP. Deformation appears to extend ~4 m above this horizon. The current study is an outgrowth of these results.

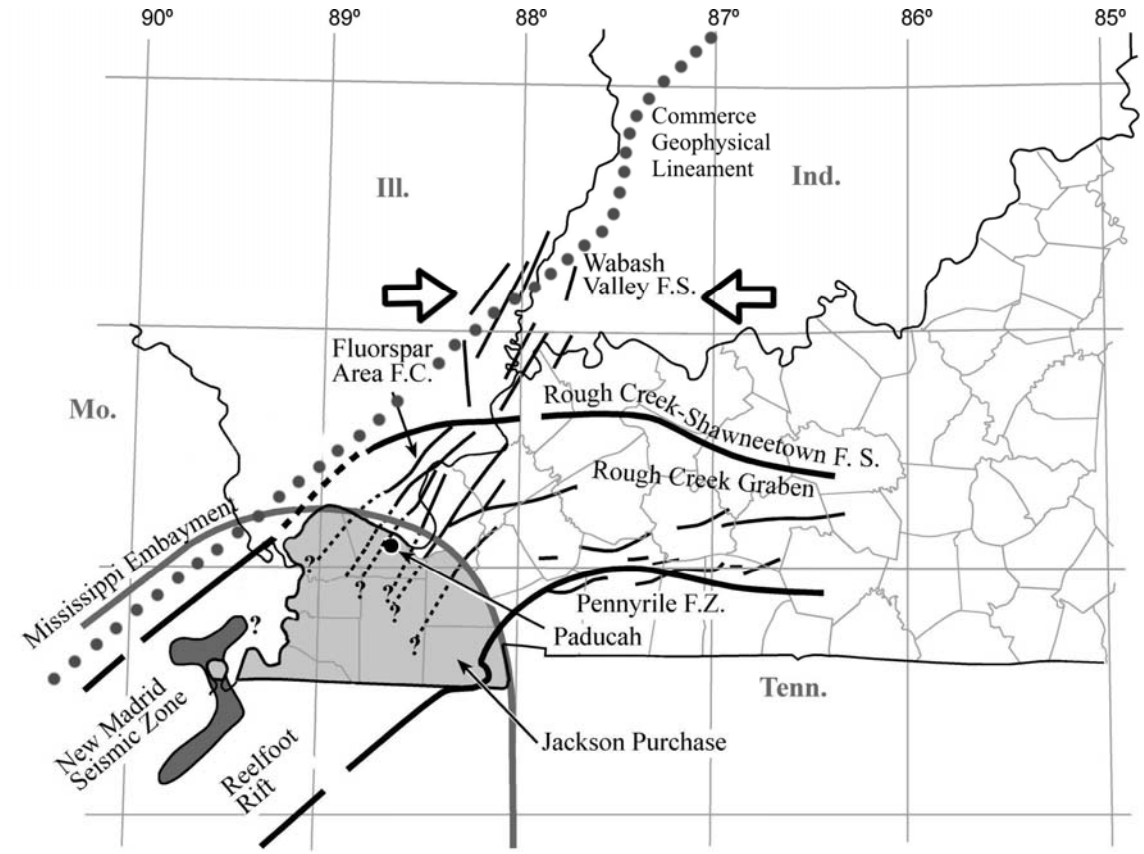

Figure 2.1 Significant structural features in the region surrounding the WVFS (modified from Kolata and Nelson, 1991). The two arrows adjacent to the WVFS show the Midcontinent stress state (Zoback and Zoback, 1980). The arc in the southwestern portion is the northern limit of the Mississippi Embayment. The dotted line is the Commerce Geophysical Limit (Hildenbrand and Ravat, 1997; Harrison et al., 1999).

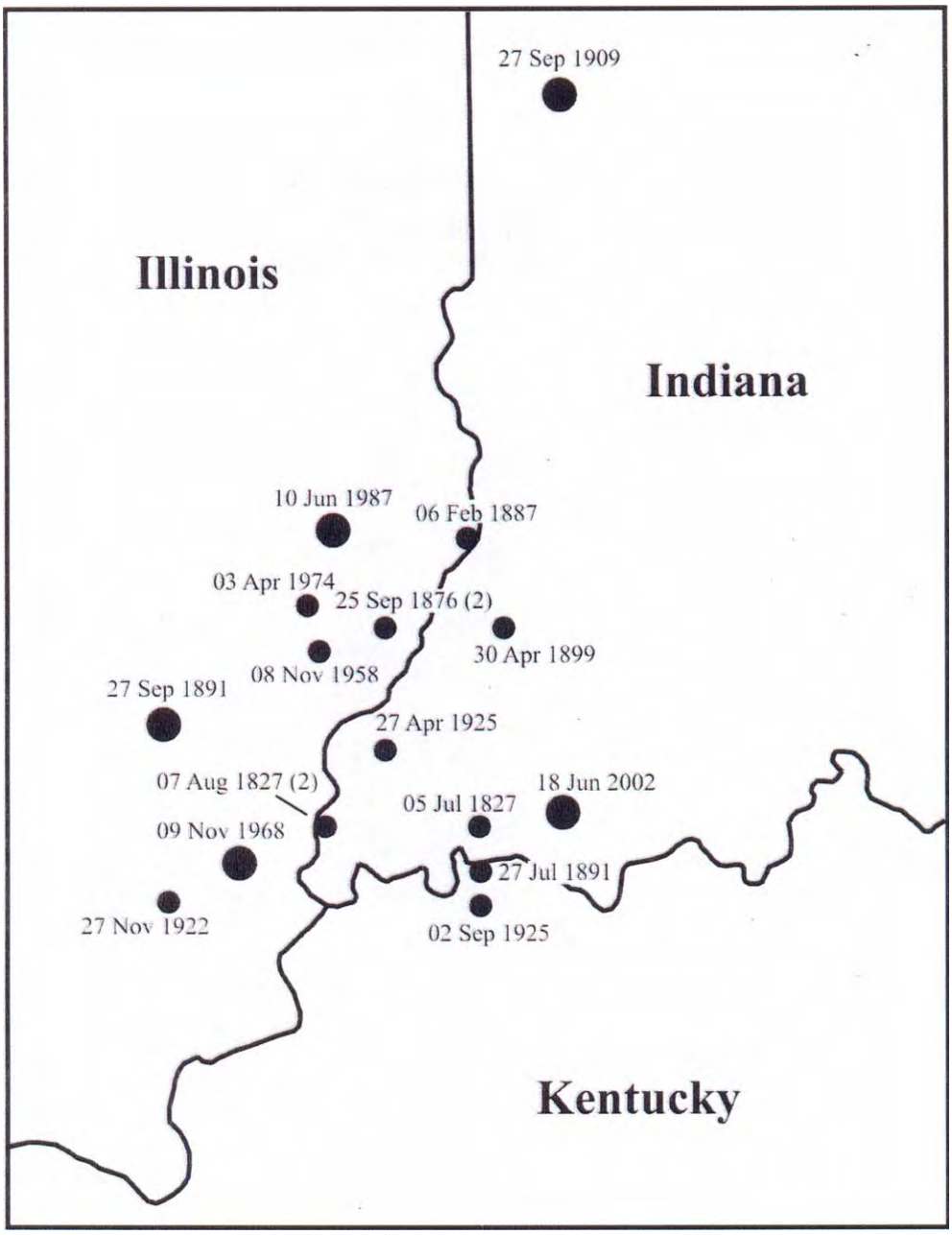

Figure 2.2 Epicenters of 18 damaging earthquakes (Modified Mercalli VI or greater) occurring since 1820 in the WVFS (modified from FMSM Engineers, 2002). Numbers in parentheses indicate the number of events.

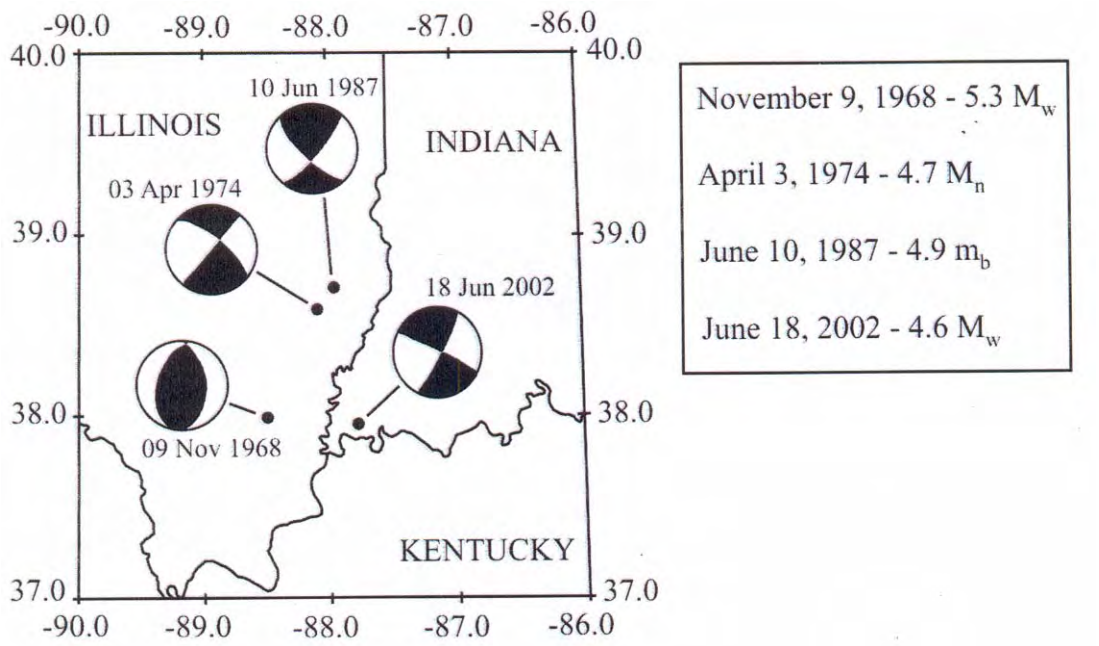

Figure 2.3 Focal mechanisms and locations for four earthquakes in the vicinity of the WVFS (Rutledge, 2004).

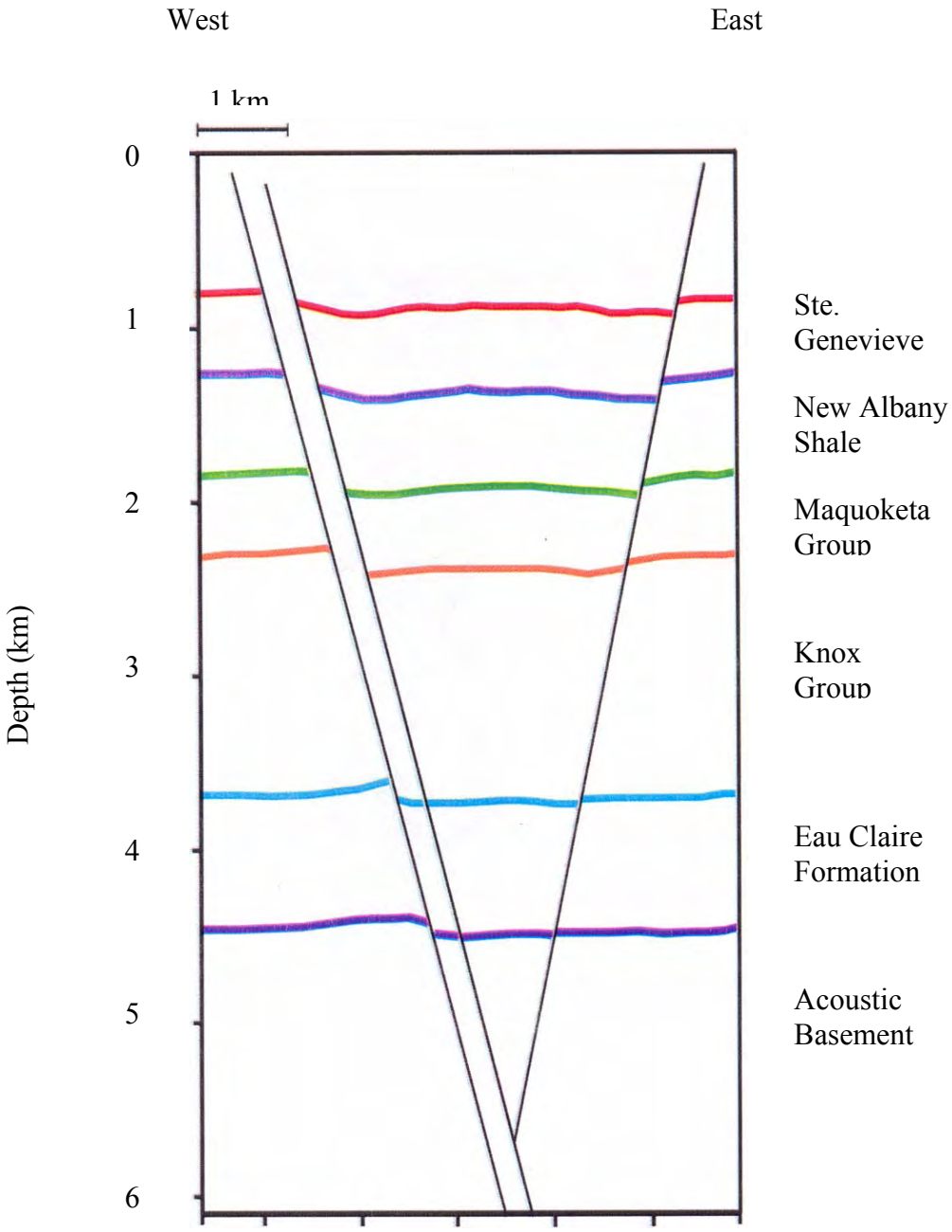

Figure 2.4 Orientation of the WIF (left) and HLF (right) with depth (modified from Rene and Stanonis, 1995; Rutledge, 2004).

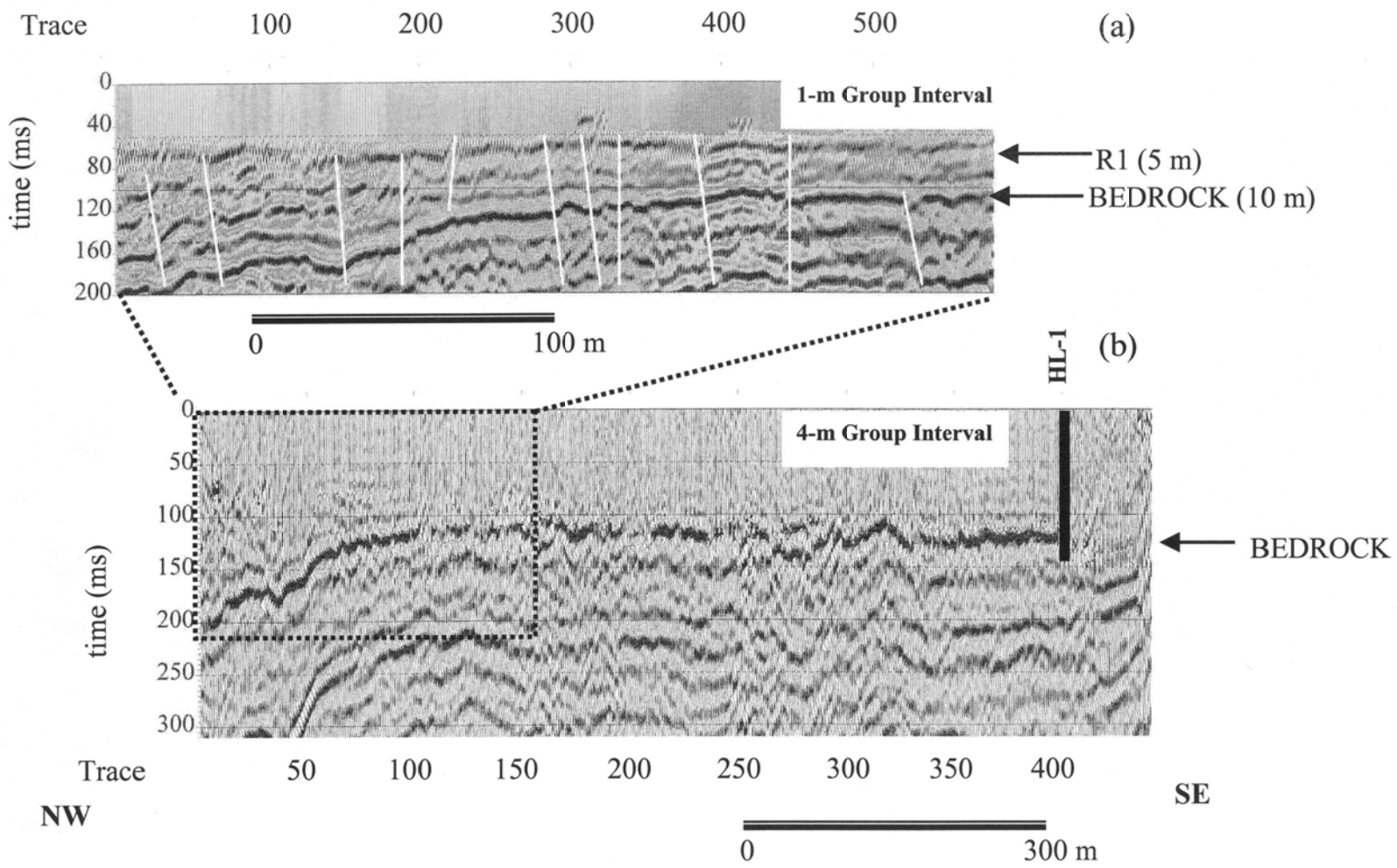

Figure 2.5 Reconnaissance and very near-surface SH-wave profiles across the southern Hovey Lake fault (Woolery, 2005).

3. Methodology

3.1. Seismic Reflection

3.1.1. Acquisition Geometry

The seismic reflection acquisition technique used in this study is the common midpoint (CMP) or common depth point (CDP). This process involves sorting traces into gathers of common subsurface sample points and stacking the gathers to enhance reflected arrivals [Stein and Wysession, 2003]. The data are sorted and stacked so that all traces corresponding to a single location will be added together. The process involves enhancing (i.e., constructive interference) primary reflections while diminishing (i.e., destructive interference) the "noise." Anything not a primary reflection is considered noise (e.g., direct, head, surface, and air waves) [Stein and Wysession, 2003]. A normal moveout (NMO) is subsequently done to "flatten out" (i.e., shift to zero-offset time) the hyperbolic signature of a reflection, which is caused by differences in offset. The NMO causes a reflection to appear at the same time for all offsets [Stein and Wysession, 2003]. Other types of waves do not have this hyperbolic shape and will not "flatten out". Traces are added together after NMO, and essentially form a trace that has zero offset between a source and receiver [Stein and Wysession, 2003]. Reflections that are added together will constructively interfere (i.e., higher amplitude); whereas, other types of waves will destructively interfere and be diminished.

Walkaway soundings were completed, prior to the seismic surveys, in order to determine the best acquisition parameters (Figure 3.1). These soundings determined which shot/group intervals and source-receiver offsets would produce the best signal-recording window. The chosen offsets are called the optimum window, which is the section of the seismogram where reflections are best isolated from coherent noise. This is an important step in obtaining quality seismic reflection data

3.1.2. P-wave Reflection Acquisition

Previous experience, as well as walkaway soundings, has shown two inline spreads of 24 Mark Products 40-Hz, vertically polarized geophones with 7.5-cm spikes spaced at 2 m intervals is an effective acquisition array. Walkaway soundings indicated that a near offset of 30 m was optimal for isolating the reflection signal window. The seismic data were collected at a sampling interval of 0.25 milliseconds (ms). A 15-Hz low-cut filter was used with the high-cut filter out. The 15-Hz filter was chosen in order to eliminate low-frequency ground roll. A 60-Hz notch filter was needed in some areas to suppress noise from unshielded power lines. Acquisition parameters can be seen in Table 3.1.

3.1.3. SH-wave Reflection Acquisition

Two inline spreads of 24 Mark Products 30-Hz, horizontally polarized geophones with 7.5-cm spikes spaced at 2 m were initially used. Site-specific conditions at the Indiana site (and experience) reduced the geophone spacing to 1 meter in order to properly image the very near-surface sediment. The seismic data were collected at a sampling interval of 0.25 ms. A 25-Hz low-cut filter was used with no high-cut filter. Again, a 60-Hz notch filter was needed in some areas to suppress noise from unshielded power lines. Acquisition parameters can be seen in Table 3.1.

3.1.4. Seismic Resolution

Traditionally, P-wave seismic-reflection methods have been used to image the neotectonic deformation that propagates into the unlithified, water-saturated fill of the alluvial valleys in the central United States [e.g., Sexton and Jones, 1986; Schweig et al., 1992; Williams et al., 1995; Odum et al., 1998; Stephenson et al., 1999]. CMP reflection surveys using the horizontally polarized shear-wave (SH) mode [e.g., Woolery et al., 1993, 1996; Harris, 1996; Harris et al., 1998] have been found to be more amenable for imaging neotectonic features in near-surface sediment (<100 m), however [Woolery, 2005]. Shear waves are superior for near-surface imaging because they are “framework waves” (i.e., not affected by the degree of water saturation), and therefore sample the geologic medium more accurately than the fluid-sensitive P-wave [Woolery et al., 2004]. SH is the preferred phase because SH signals are easy to identify, unlike SV (vertically

polarized shear wave) signals, because of the lack of mode conversion at the refracting and reflecting boundaries. The lower velocity S-mode also shifts the optimal acquisition window to the nearer offset, and expands the spatial and temporal optimal window (Figure 3.2). The increased temporal window allows easier, more accurate identification of the reflecting boundaries, as a result of the increased separation of the signal and coherent noise events. Furthermore, the broader spatial window at the near offset permits application of increased fold without introducing adverse wide-angle-reflection effects. In addition, experience shows that although S-waves commonly have frequencies only one-half to one-third that of P-waves, the P-waves have velocities five to 10 times higher than S-waves [Woolery et al., 2004]. Consequently, it is estimated that resolution can be improved by a factor of 2 to 3 through the use of S-waves [Woolery et al., 2004]. This is because resolution is related to wavelength, which is a function of velocity divided by frequency. This is a very important point when considering small fault displacements (i.e., 1 to 3 m) and investigating relatively thin low-velocity media [Woolery, 2005]. The SH-wave data has average velocities ranging between 240 and 360 meters per second, and a dominant frequency of approximately 40 Hz [Woolery, 2005]. Therefore, the temporal resolution (i.e., calculated using the one-quarter wavelength criteria of Sheriff and Geldart [1989]) ranges between 1.5 m in the very near surface and 2.2 m at the top of bedrock [Woolery, 2005]. The limits of detection are considerably smaller (i.e., 1/10 λ to 1/20 λ) [Woolery, 2005]. The spatial resolution of a feature is constrained between approximately two and four shotpoints, based on the radius of the first Fresnel zone [Woolery, 2005].

3.1.5. Acquisition Equipment

3.1.5.1. Seismograph

All seismic reflection data (P and SH-wave) were collected with a 48-channel Geometrics StrataVisor® seismograph. The seismograph is a 24-bit system with an instantaneous dynamic range of 120 db that stores data on an internal hard drive. It contains floating preamp gains with a maximum of 48 dB. Furthermore, the seismograph has zero-phase digital anti-alias filter that is automatically selected for each sample rate (e.g., –3dB corner frequency at 82% of Nyquist frequency, down 130 dB at Nyquist). The stacking

trigger accuracy is +/- 1/128 of the sampling interval, and the timing accuracy is 100 ppm.

3.1.5.2. Geophones and Takeout Cables

The P-wave geophones used in this study are Mark Products 40-Hz, vertically polarized geophones with 7.5-cm spikes. The SH-wave geophones are Mark Products 30-Hz, horizontally polarized geophones with 7.5-cm spikes. The SH-wave geophones were all oriented in the same direction and leveled when planted. All geophones were planted firmly into the sediment. Both types of geophones were connected to Mark Products takeout cables with takeout spacings of 1 or 2 m. These cables contained 24 takeouts and were always used in pairs to produce 48 channel seismic data.

3.1.5.3. Energy Sources

P-wave energy sources available for the near-surface profiling included vibratory and impact. The most efficient source of those available for very near surface imaging was an impact source (i.e., an 8-inch square steel plate struck vertically with a 10-pound sledgehammer). The steel plate was placed on flat asphalt that was free of debris, in order to produce higher frequency (i.e., higher resolution) data than would be possible on softer surfaces (e.g., gravel, unconsolidated sediments, etc.). Less consolidated surfaces allow more attenuation to take place in the near surface and more surface wave energy to develop. The placement of the plate was 30 m from the inline spread and constant throughout. Three impacts were created and stacked at each shot point.

S-wave energy sources available for the near-surface profiling included vibratory and impact. The most efficient source of those available for very near surface imaging was a section of steel H-pile struck horizontally with a 1.4 kg hammer. The hold-down weight of the H-pile was approximately 70 to 80 kg, including the weight of the hammer swinger and the H-pile section [Woolery et al., 2004]. The flanges of the H-pile were placed and struck perpendicular to the geophone spread for SH-mode generation. The H-pile was placed in prepared slit trenches to resist movement and improve the energy input into the ground [Woolery et al., 2004]. The orientation of the sensor is parallel to the direction of

the hammer swing. The setup is shown in Figure 3.3. Polarity reversals and impacts of the sledgehammer on both sides of the energy source were recorded to optimize SH-wave energy [Woolery et al., 2004]. The overall signal interpretation was corroborated using preliminary walkaway soundings. Geophones in the two inline-spreads were spaced at 1 or 2 m intervals, for a total spread length of 48 or 96 meters, respectively. In general, the hammer blows were stacked three to six times per shotpoint.

3.1.6. Data Processing

Data processing was performed on a Pentium-IV based microcomputer using VISTA 7.0® (Seismic Image Software, 1995), commercially available software package for seismic signal processing. A conventional shallow CDP processing sequence was applied to the data [Baker, 1999]. The general processing steps are shown in Figure 3.4. Muting was given special attention to ensure that coherent noise (i.e., refractions, ground roll, air wave, etc.) was not inadvertently stacked. Example field files along the survey are shown (Figure 3.5).

3.1.7. Interpretation

Structural interpretations of all seismic profiles are based on: (1) offset reflectors, (2) abrupt termination of relatively strong reflection horizons, and (3) changes in reflector apparent dip [Woolery, 2005]. These imaged features can also result from non-tectonic processes (e.g., slumps, lateral spreading, collapse features, facies change, etc.), but temporal replication and constraints from well-log-derived bedrock structure maps in the area can constrain the interpretation. Furthermore, all interpreted anomalies extend to the base of their respective profiles and are therefore interpreted as structural features. Noticeable sediment thickening on the downthrown side of an interpreted fault can also be a structural indicator.

The wide-angle reflection associated with seismic data limits vertical and horizontal resolution. Near-surface reflections occur deeper than their true depths because of greater angles of reflection and the associated travel times. In addition, lateral velocity variations can create apparent dips and offsets. Phase changes can also occur and

decimate the signal during the stacking process. Lastly, high amplitudes result from a lack of transmission associated with incidence at angles greater than the critical angle. Because of these effects, there is error associated with velocities and depths. These potential problems must be considered when interpreting seismic data.

3.2. Coring

Potential neotectonic deformation targets were located with seismic reflection techniques, and intrusively drilled to complete sampling the near surface (< 7 m depth). The purpose of the coring was to define the stratigraphy affected by near-surface faults, and correlate to the SH-wave reflection profiles. In addition, the core holes were used to collect organic material (charcoal and shells) from various horizons to constrain neotectonic timing, by carbon dating methods.

For seismic hazard assessment, the most relevant stratigraphy is likely confined to the upper part of the record; therefore, the borings were limited to the upper 6.5 meters of sediment. The existing geotechnical boreholes in the area were used to constrain the thickness of the complete Quaternary section. Twenty-nine cores were obtained; the core-hole spacing ranged between 10 and 20 m. Drilling was done coincident to the seismic lines. Drilling concentrated over the most significant anomalies interpreted on the seismic profiles. The stationing at each site corresponded to the seismic shotpoints, and located from surveyed landmarks.

All core holes were sampled continuously from the ground surface to their terminal depth using a Giddings Soil Sampler (Figure 3.6). The truck-mounted soil sampler used a hydraulic system to move a rotary head that was connected to a kelly bar. The soil sampler was positioned over a coring target and the trailer anchored to the ground. A baseplate and a leveled kelly bar keep the soil sampler fixed and vertical. A drive rod was locked into the rotary head and attached to a soil tube. A soil tube and rod(s) are extended into the undisturbed subsurface, retracted, and the soil sample removed. We placed the soil samples in sections of PVC tubing halved lengthwise. A soil length (1.27 m) was extruded with any losses noted. Multiple sampling tubes were used and sprayed with a lubricant to help extrude the samples.

The cores were split lengthwise and logged. The classification and correlation were based on separation of cores into units with like characteristics: grain size, color, and the presence of any other diagnostic characteristics (e.g., mottling, fossils, clasts, etc.). Colors were defined by the Munsell color system [www.munsell.com]. The depths to each unit boundary were recorded using a steel tape.

3.4. Carbon Dating

The organic material that was collected during the coring operations was sent to Beta Analytic Radiocarbon Dating Laboratory. The organic material consisted of charcoal and/or shells. Small material amounts were dated using accelerator-mass-spectrometry (AMS) radiocarbon dating. The charred material was pretreated with acid, alkali, and acid again. The shelly material was pretreated with an acid etch. The ages presented in the results are conventional radiocarbon ages as opposed to measured radiocarbon ages, but the two are similar. The conventional ^{14}C age includes $^{13}C/^{12}C$ corrections and is the most appropriate radiocarbon age. More details of the carbon dating procedure and results are located in Appendix A.

Table 3.1 Seismic reflection acquisition parameters (P- and SH-wave).

Location	P-/SH-wave	Near Offset (m)	Shot Interval (m)	Geophone Spacing (m)	Record Length (s)	Sample Interval (ms)	Acq. Filter: Low Cut (Hz)	Acq. Filter: High Cut (Hz)	Geophone (Hz)
Caborn	P	30.0	2.0	2.0	1.024	0.25	25	out	40 Hz
Caborn	SH	1.0	1.0	1.0	1.024	0.25	25	out	30 Hz
Hovey Lake	SH	2.0	2.0	2.0	1.024	0.25	25	out	30 Hz

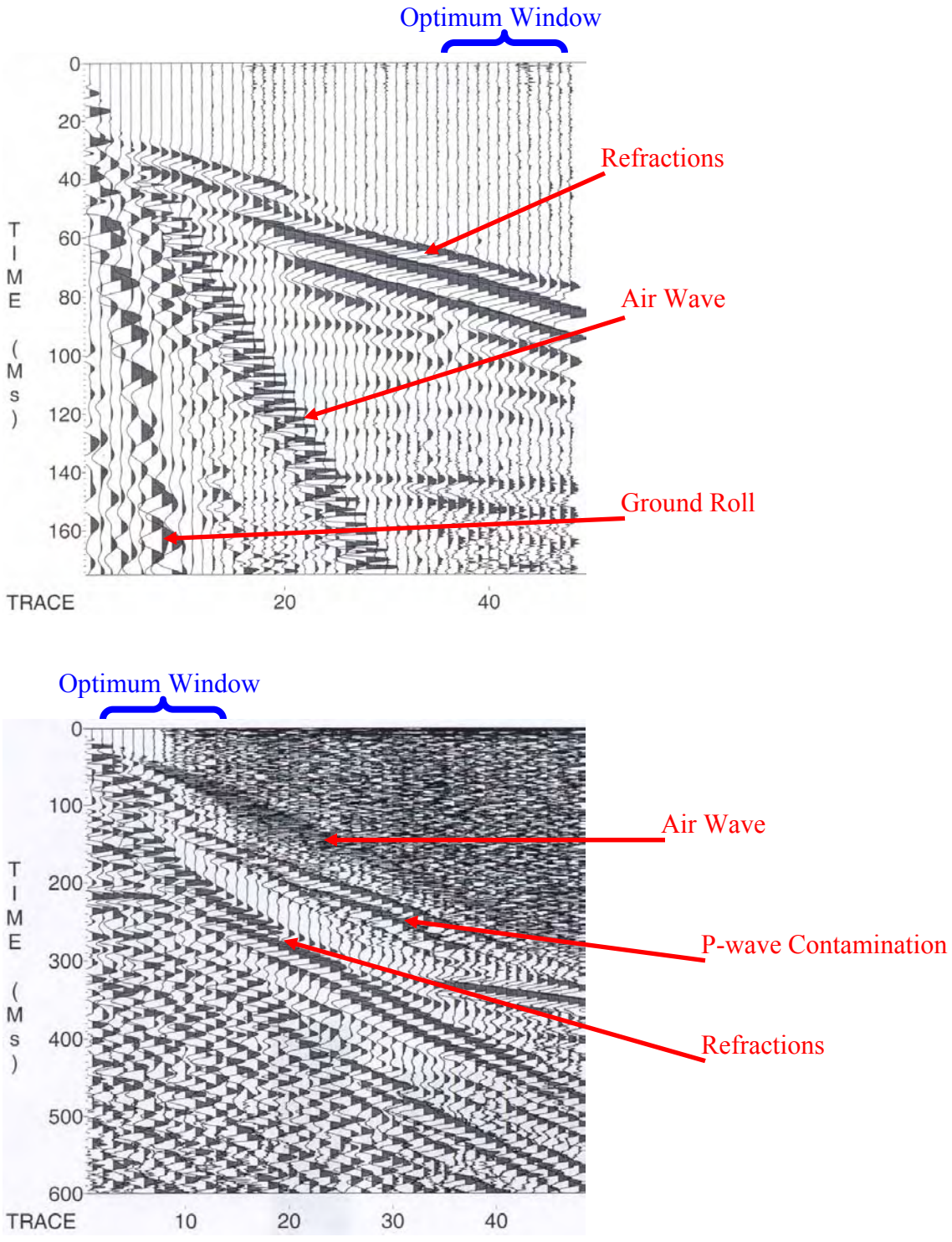

Figure 3.1 Walkaway tests from the Caborn site: (Top) P-wave, (Bottom) SH-wave. Data was contaminated by P-waves because polarity reversals were not used.

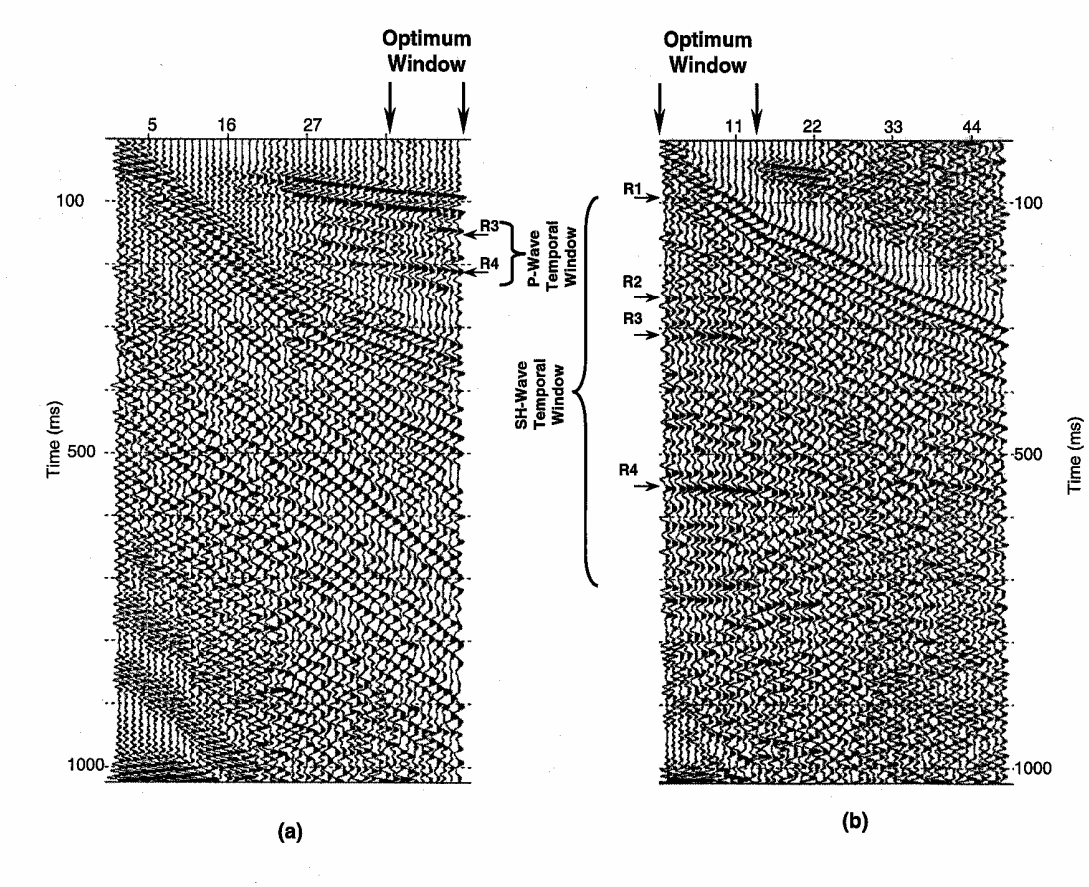

Figure 3.2 Optimum recording windows from previously acquired (a) P-wave and (b) SH-wave walkaway tests. The comparison demonstrates the superior nature of the SH-wave technique in the near-surface environment (Woolery and Street, 2002).

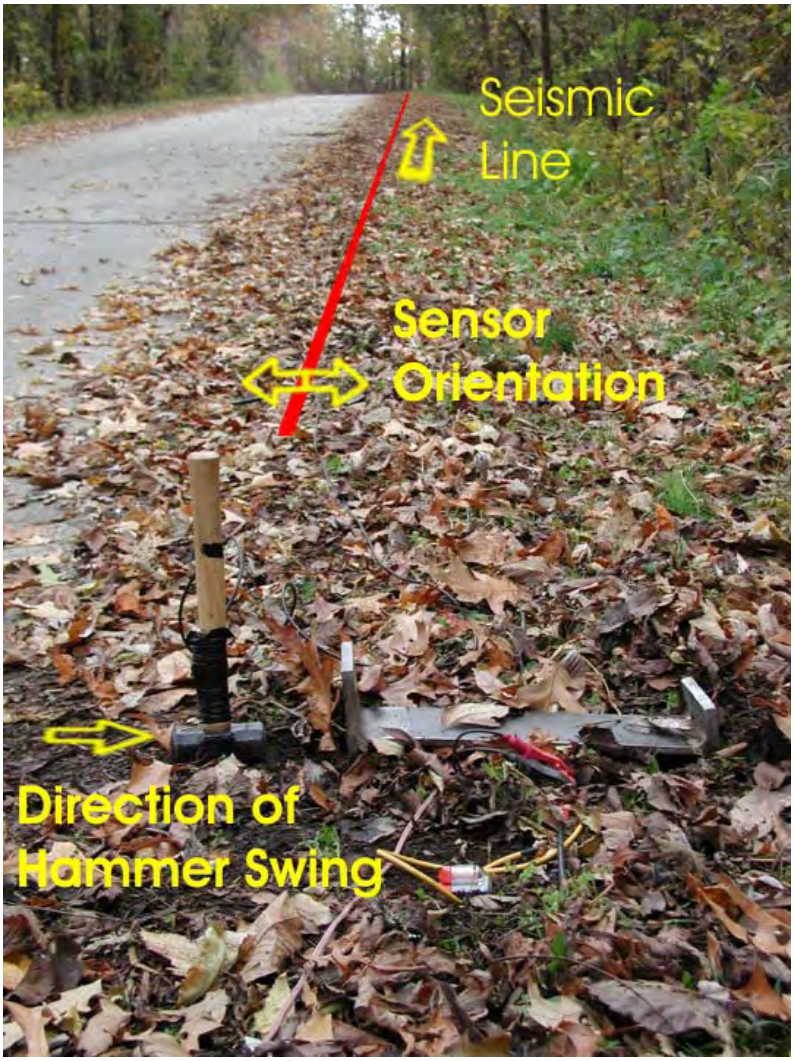

Figure 3.3 Relative orientations of spread, sensor, and hammer swing for SH-wave data acquisition. Steel H-pile and horizontally polarized geophone are located near the bottom (Rutledge, 2004).

1) **Reformat .SGY**
2) **Spherical divergence gain**
3) **Mean gain**
4) **Band-pass filter**
5) **AGC (100 ms)**
6) **Kill bad traces**
7) **Mutes**
8) **Velocity analysis**
9) **NMO correction**
10) **Brute CMP stack**
11) **Residual statics (10 ms)**
12) **Final CMP stack**
13) **Post-stack FK-filter**

Figure 3.4 Signal processing procedures.

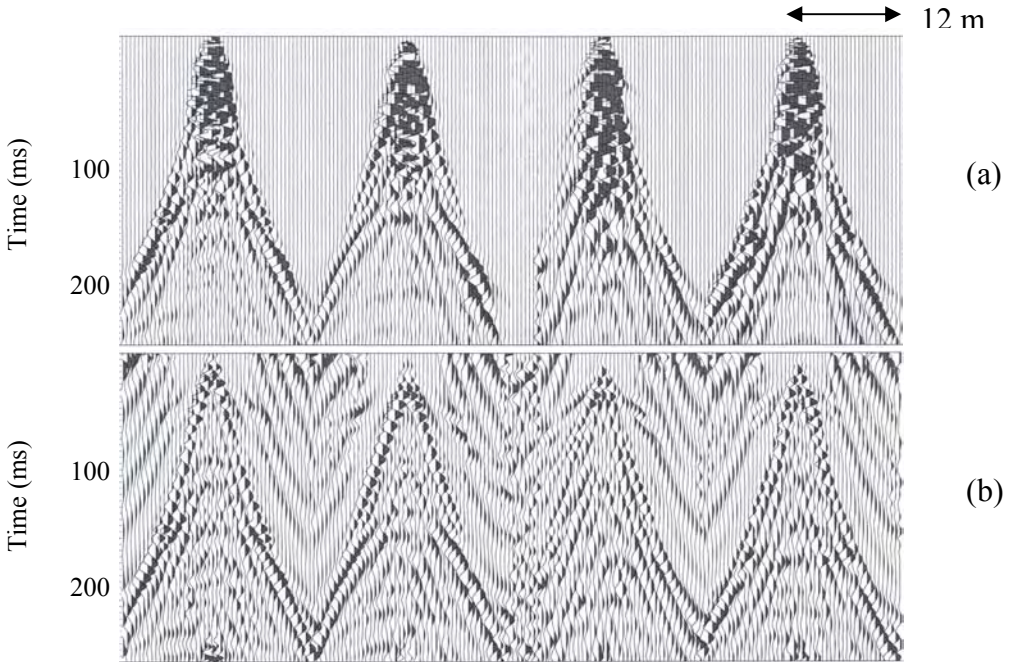

Figure 3.5 Example field files (0-250 ms) from four locations in the Caborn SH-wave profile that show various steps in the processing scheme: (a) raw, (b) band-pass filtered with automatic gain control. The beginning of the third record in (a) and (b) contains some dead traces due an inability to plant geophones (bridge crossing).

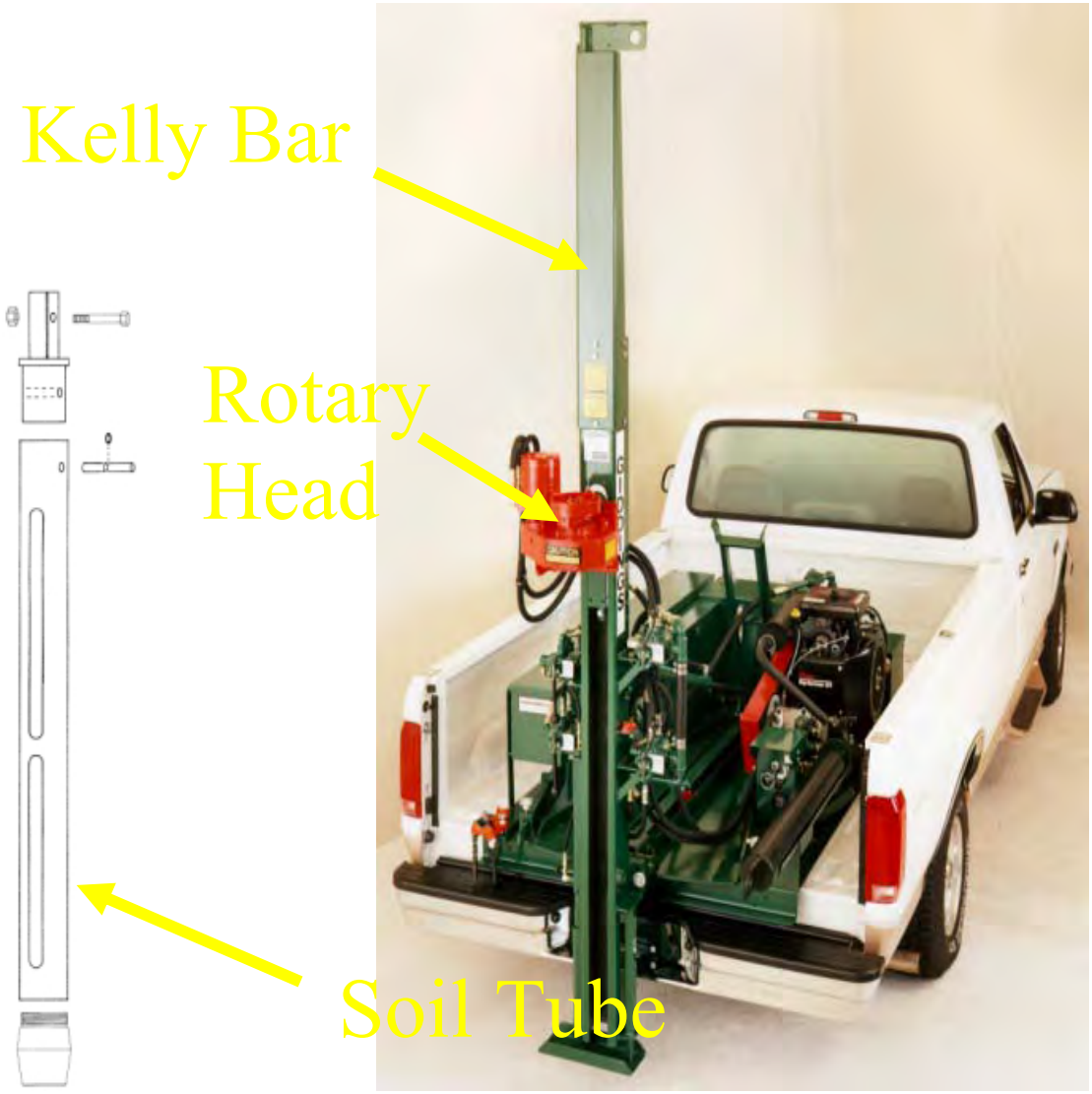

Figure 3.6 Truck-mounted Giddings Soil Sampler and soil tube that are very similar to those used in the coring projects (www.soilsample.com).

4. Results and Interpretation

4.1. Caborn Site

4.1.1. P-wave Profile (C1)

The Caborn site is located approximately 2.5 km north of Indiana State Route 62 and around 8 km northeast of the city of Mount Vernon, IN. The line was shot on the south side of 600 East. The first shot point was located ~26 m east of the eastern bridge abutment. The bridge is immediately west of the intersection of roads 600 East and 500 South.

The P-wave seismic reflection technique was used for reconnaissance to locate the bedrock expression of the Caborn fault(s). The uninterpreted profile is shown in Figure 4.1. The main part of the profile contains 730 traces (i.e., 730 m long) and is oriented from west-to-east (0-730). The upper limit of the data is approximately 55 ms two-way travel time (TTT), and it corresponds to a depth of 35 m based on velocity model calculations. Similarly, reflections are visible to a depth of ~140 ms TTT, corresponding to a depth of ~120 m. A second section was acquired 176 m east of the first in order to avoid an active railroad. This second west-east-oriented profile is 214 m long and is shown in Appendix B. The vertical exaggeration for both profiles is ~2.

A significant deformation zone was imaged along the profile that coincides with the CF's mapped location determined from well logs. The deformation extends from approximately trace 92 to 317, 225 m wide. The main fault (or area of greatest deformation) is located at trace 195 and is designated as C1-1 (Figure 4.2). The interpreted faults along profile C1 are labeled 1, 2, and 3. The C1 profile exhibits layers that have apparent dips in opposite directions on either side of the main fault. The apparent dip slopes toward the fault on each side. The dip magnitude is greatest immediately adjacent to the fault. In the deformational area, there are varying directions and degrees of dip, as well as some minor offsets (~2 m). In addition to the change in dip, a fault is interpreted by a loss of coherency and displacement. The lack of coherency near the fault is interpreted to be a result of the highly deformed rock. C1-1 is near vertical with a slight easterly dip. The C1-1 displacement is down to the east. In the

footwall, the top of the undeformed bedrock is at a depth of approximately 35 m. Undeformed bedrock in the hanging wall is at a depth of ~40 m; therefore, the CF has a bedrock offset of ~5 m. This amount of offset is also visible immediately across C1-1. The fault also extends above Paleozoic bedrock into the Quaternary sediment cover. Similar offset is seen on all the overlying imaged reflectors. Therefore, fault movement is interpreted to be predominantly normal or involves strike-slip movement of sections with little or no dip.

Since its formation in an extensional regime, the CF has likely been reactivated through transpressional motion as inferred from the contemporary stress state. Offset that was produced during normal faulting may have been diminished by later episodes of reverse and/or strike-slip motion. Recent fault movement is thought to be primarily strike-slip from focal mechanism studies [Kim, 2003].

The second fault (C1-2) is located at trace 50. The fault has an apparent dip of ~85°, downthrown to the west. The offset at bedrock is approximately 2 m. The top of bedrock in the hanging wall occurs at a calculated depth of ~50 m depth. The amount of offset is similar along the overlying reflectors as well. This offset can be traced to the upper limits of the profile. Furthermore, reflectors on the west side of the fault are horizontal, whereas those to the east have an apparent easterly dip.

Fault 3 (C1-3) is at trace 500. The evidence for C1-3 includes abrupt changes in the directions and amounts of dip of the imaged layers, which is visible in an approximately 40 m wide zone centered at the fault location. The general trend of the bedrock reflector to the east of C1-3 has an apparent dip that is down westward; whereas, the bedrock reflector to the west of the fault is essentially horizontal. The amount of offset at bedrock is 1-2 m. The amount and direction of displacement is similar below bedrock, to the base the section. The reflectors imaged above bedrock do not show noticeable offsets.

An anticlinal feature is interpreted at a depth of ~100 m (in the lower limits of the data) centered near trace 550. This feature has varying directions and degrees of dipping reflectors.

4.1.2. SH-wave Profile (C2)

Profile C2 is a 208 m long SH-wave profile collected coincident to traces 98-305 from the P-wave profile (oriented west to east). The uninterpreted profile (C2) is shown in Figure 4.3. The upper limit of the data is calculated at ~4 m depth. The top of bedrock occurs between ~25 and 34 m depth. The lower limit of the data corresponds to a maximum depth of 50 m. The vertical exaggeration in this profile is ~1.4.

There is considerable difference between depth calculations for the P-wave and SH-wave profiles. Bedrock in the footwall occurs at depths of ~35 m and 30 m for P-wave and SH-wave data, respectively. This is an error of ~17% that results from inaccurate velocity picks. The velocities are estimated from hyperbolic curve matching; however, the low fold data (i.e., 12 traces) at a small bin size (i.e., near the hyperbolic apex) cause a broad range of velocities to satisfy the curve match.

The SH-wave profile shows deformation in 3 zones (Figure 4.4). Displacement is exhibited along the most coherent soil reflector (highlighted yellow) and the Paleozoic bedrock (highlighted blue), as well as various other discontinuous reflectors. The dominant structure in the profile (C2-1) is located at trace 265. The presence of the fault is interpreted from a lack of coherency, offset of strata, diffraction patterns, and a change in reflector dips. The Quaternary reflector around 210 ms TTT loses coherency and then is visible again at approximately 224 ms TTT. These reflectors correspond to depths of ~12.1 and 13.2 m, respectively. This is interpreted as a normal fault, with ~1.1 m of offset immediately across the fault. The amount of offset across the fault is similar at the top of bedrock. In a larger zone (between traces 250 and 415) there is a bedrock offset of ~4 m. In this larger zone, the previously mentioned soil reflector (210 and 224 ms TTT) is offset by ~2 m. The hanging wall is downthrown to the east, and the apparent orientation of the fault is near vertical. This location and structure is consistent with

previous mapping and imaging done by other researchers (e.g., Rutledge, 2004; Woolery et al., 2004; Woolery, 2005). This fault correlates with the primary fault imaged with the P-wave C1-1 profile (Figure 4.2). The reflectors adjacent to the faults show similar dips in the two profiles, as well. Offset is visible to the upper limit of the SH-wave data, and C2-1 is interpreted to extend to the upper limit (~4 m depth). Diffraction patterns are visible as series of coherent noise with large degrees of dip, especially to the east of the fault. Diffraction pattern locations are controlled by where discontinuities in boundaries (i.e., horizons) occur. The degree of diffraction dip is a function of the interval velocity. Furthermore, reflectors are primarily flat to the west of the fault, but immediately to the east they show a slight dip down to the west. At the surface, above the fault location, there is a drainage ditch ~3 m deep that is spanned by a bridge. A small stream is oriented NNE, and it is possible that the stream location has been influenced by past faulting.

Another location of normal faulting (C2-2) is evident at trace 105. This location shows a small amount of offset (~1 m or less) and a loss of coherency. This small amount of offset is interpreted as a minor structure. The displacement has a down throw to the west and the fault is near vertical. Another area that shows a loss of coherency, offset of strata, and change in reflector dips is at trace 140 (C2-3). The amount of offset is also small (1 m or less). This fault is near vertical and shows down to the west offset along soil reflectors. The area that is located between the faults shows various directions and degrees of dip. Reflector dips are pronounced on the west side of C2-3's bedrock expression. Both of these faults show a loss of offset or a slight inversion of offset deeper in the profile. This is interpreted to be the result of strike-slip motion. This could possibly be an offset erosion surface instead.

4.1.3. Coring

Eight cores were collected from two areas of deformation defined by the initial seismic profiling. The cores ranged in depth from 4-6.5 m and sampled the part of the near surface that was not imaged with the seismic lines. At the Caborn site, core 1 was drilled within a meter of trace 150, from the P-wave seismic line. Core 2 was located 20 m east

of core 1. The third core was located 20 m east of core 2 and coincides with the location of the primary faulting observed on the P-wave profile. Two more cores (4 & 5) were taken from locations 20 m east of the previous core. Three cores were taken from a secondary area of proposed deformation. Core 6 coincided with trace 60 from the P-wave profile and was located 10 m east of the second proposed fault location. Core 7 was located 10 m west of this fault, and the final core (8) came from a location 10 m west of core 7 (Figure 4.5).

Determining the extent of faulting was difficult, in most locations, due to a lack of stratigraphy. The cores were composed almost entirely of clay with a thin cap of silt. Changes in color and the degree of mottling were used to differentiate between different layers. A shelly layer was used as a marker bed because it was unique and present in all the cores. The top of this layer was found at depths of ~3.4-4.4 m in cores 1-4 and 6-8. Furthermore, the depth to the top of this layer ranges from 4.25-4.45 m in cores 1-4. In core 4 it was encountered at 4.4 m depth; however, in core 5 this marker bed was not encountered until ~5.7 m depth. This is interpreted to be the result of faulting (~1.3 m of offset). The midpoint between cores 4 and 5 corresponds to the main fault location in the SH-wave profile. Furthermore, the amount and style of offset matches what is seen in the SH-wave profile. The interpreted fault location is shown as a red line in Figure 4.5.

Three organic samples were collected from the upper five meters of sediment. Only two were of sufficient quantity for accelerator-mass-spectrometry (AMS) Carbon (^{14}C) dating. One organic sample (shelly material) yielded a ^{14}C age of 19740 +/- 110 YBP from a depth of 4.53 m. This date is consistent with other ages measured in the region (e.g., Rutledge, 2004; Woolery et al, 2004; Woolery, 2005). The displacement interpreted in the coring data suggests faulting extends to 4.4 m depth or shallower. This results in evidence of fault activity within the last 20,000 YBP. Therefore, this fault should be considered "capable," based on the classification by the U. S. Army Corps of Engineers and the U. S. Nuclear Regulator Commision (i.e., movement on the fault within the last 35,000 years). The other organic sample (charcoal), which was able to be dated, came from a depth of 1.13 m and produced an age of 540 +/- 50 YBP. No offset

was found at this elevation, however. The stratigraphy in the uppermost part of the cores does not allow the vertical extent of faulting to be determined. GPR has been considered for this site, but high clay content limits its effectiveness. A trenching project is required to assess the structure's temporal extent.

4.2. Hovey Lake Site

4.2.1. SH-wave Profile (HL1)

A SH-wave profile was acquired across the HLF. The seismic line was located less than 300 m from the southern bank of the Ohio River, in Henderson County, KY. This location is immediately across the river from Mount Vernon, IN. The line was collected along an unimproved road that is nearly parallel with the river. The uninterpreted profile is shown in Figure 4.6. The profile is 970 m long and oriented from west to east (0-970). The data is continuous below a calculated depth of ~5.25-6.75 m. Calculations from this profile's velocity data allow 400 ms TTT to be converted to a depth of 35 m. Below 400 ms TTT there is a lack of velocity data, but the base of the profile (500 ms TTT) likely corresponds to a depth of ~50 m. The vertical exaggeration in this profile is ~7.

The bedrock expressions of the northern HLF fault were located in the profile around traces 314 and 343 (HL1-1). Bedrock is interpreted as the high-amplitude, coherent doublet seen between 300 and 350 ms TTT. The bedrock is highlighted blue in Figure 4.7. The velocity characteristics suggest the top of bedrock is at a depth of ~25 m. The imaged fault location agrees well with the mapped location derived from a large number of petroleum borings in the immediate area. The HLF is interpreted to be listric in the upper section of the subsurface (< 50 m depth). In addition, the fault strand that dips down to the west is interpreted as the one that extends to a greater depth. Depth calculations from undeformed areas on both sides of the fault (trace 20 & 480) show down to the west offset of ~1.5 m. The location of HL1-1 in the profile was determined based on a noticeable offsets of bedrock and losses of coherency. The fault strands form an offset zone that is approximately 30 m wide. The amount of offset between reflectors that are inside and outside of the deformation zone is approximately 2.5 m. Further evidence for this fault location comes from the change in dip of bedrock. The general

trend of dip is up eastward on the west side of the fault and down eastward on the eastern side. Another coherent reflector which occurs at approximately 250 ms TTT shows a similar change in dip. This reflector is disturbed in the area of interest by an interpreted channel cut, however. The data quality is not good enough to determine if channel bottom is offset.

The channel feature is large, laterally covering most of the profile. It appears to extend from trace ~180 to ~760; however, it is possible that the channel is being imaged at an oblique angle and is much narrower in orthogonal cross-section. The channel covers a large part of the profile in the time (depth) dimension as well. Its base continues down past 250 ms TTT (~20 m depth). It extends down close to bedrock in the area of greatest interest (area of primary faulting). This limits the interpretation of the vertical extent of faulting. There is not clear evidence for displacement of the channel margin, but this is primarily a due to lack of coherent reflectors in the area of interest. Within the main channel are many smaller erosional features, but there is again no clear evidence for displacement.

The bedrock appears disturbed in other areas, but displacement is minor. Two such areas (HL1-2 and HL1-3) occur at traces 575 and 635. The bedrock imaged in this profile shows various directions and degrees of dip that are interpreted to result from deformation. These dip changes and losses of coherency further support the fault locations. HL1-2 and HL1-3 have bedrock expressions that show normal offset, down eastward, and are near vertical. The amount of reflector displacement is ~1 m at bedrock for both of these faults, so they are considered minor features. The coherent reflector above HL1-2 (~250 ms TTT) is interpreted to be slightly offset (down eastward <1 m), and it shows a change of dip direction. Therefore, the fault is interpreted to extend to the region between 200 and 220 ms TTT (15-17.5 m depth). HL1-3 is interpreted to offset (<1 m) the coherent reflector at 235 ms TTT in the opposite direction of the bedrock displacement. This is also a loss of coherency at this fault location. The change in magnitude and direction of offset along HL1-2 and HL1-3, respectively, is possibly an out-of-plane effect associated with a strike-slip component of motion.

Two more fault locations have bedrock expressions at trace numbers 840 and 935. These are interpreted as HL1-4 and HL1-5, respectively. HL1-4 is near vertical and shows a range of offsets (~1 m), down westward. There are also significant changes in the direction and degree of dip that correspond to this location. HL1-5 is also near vertical, and the offset at bedrock is ~2 m. The offset along HL1-5 diminishes towards the surface but continues to the overlying coherent reflector (255 ms TTT), at least.

In addition, there is some subtle folding throughout the area outside the channel. This can be seen along much of the bedrock reflector. The area above bedrock and outside of the channel appears to contain some minor folds as well. These structures could also be the result of erosion of lateral velocity variations. Folding is interpreted in many narrow, localized areas (wavelengths < 20 m and amplitudes of 1-2 m), as well as on a larger scale. Larger scale folds are interpreted to have wavelengths of 50-100 m and amplitudes of 4-5 m. Folding is consistent with transpressive reactivation.

4.2.2. Coring

At the Hovey Lake site, 10 cores were collected from a 185-m-wide zone that contains the main areas of proposed faulting. The first drilling location was chosen at trace 370 of the SH-wave profile. The next two cores (2 & 3) were located 15 and 35 m to the east of core 1, respectively. Core 4 was drilled 20 m east of core 3 and was located at one of the proposed fault locations. The next two cores, 5 and 6, were each drilled 20 m east of the previous core. Core 7 was drilled 28 m east of core 6, which is within approximately 2 m of the proposed fault. Three more cores (8-10) were each recovered 20 m east of core 7.

The interpreted coring data are shown in Figure 4.8. The yellow lines are used to correlate between the cores and separate units of like characteristics. The vertical yellow line represents an interpreted channel margin, but is equivocal. This margin correlates well with a small channel feature that is present near trace 400 in the SH-wave profile, however.

The upper part of each core was made up of 0.5 m or more of silt, which was underlain by sand layers ranging from 0.1 to almost 1 m thick. Most of the cores contained 2 m or more of clay and silt beneath the sand layers. Below the clay and silt, the cores were predominantly sand. There was considerable variation in thickness of (1.5 m) and depth to (2 m) different layers throughout the series of cores. This variation is attributed to the erosional structures in the sediment.

Core depths ranged from approximately 4.75 to 6.15 m. As a result, the coring sampled almost all of the area that overlies the upper limit of the seismic data. Cross sections of these cores correlate well with the channel feature. The margin of a small channel, interpreted from the core data, is visible in the seismic profile between traces 400 and 425. The lack of uniformity between the core lithologies and the presence of the channel makes it difficult to determine if faulting extends into the near surface (Figure 4.8). A charcoal sample was collected from this site also, but it was too small to be ^{14}C dated by the laboratory.

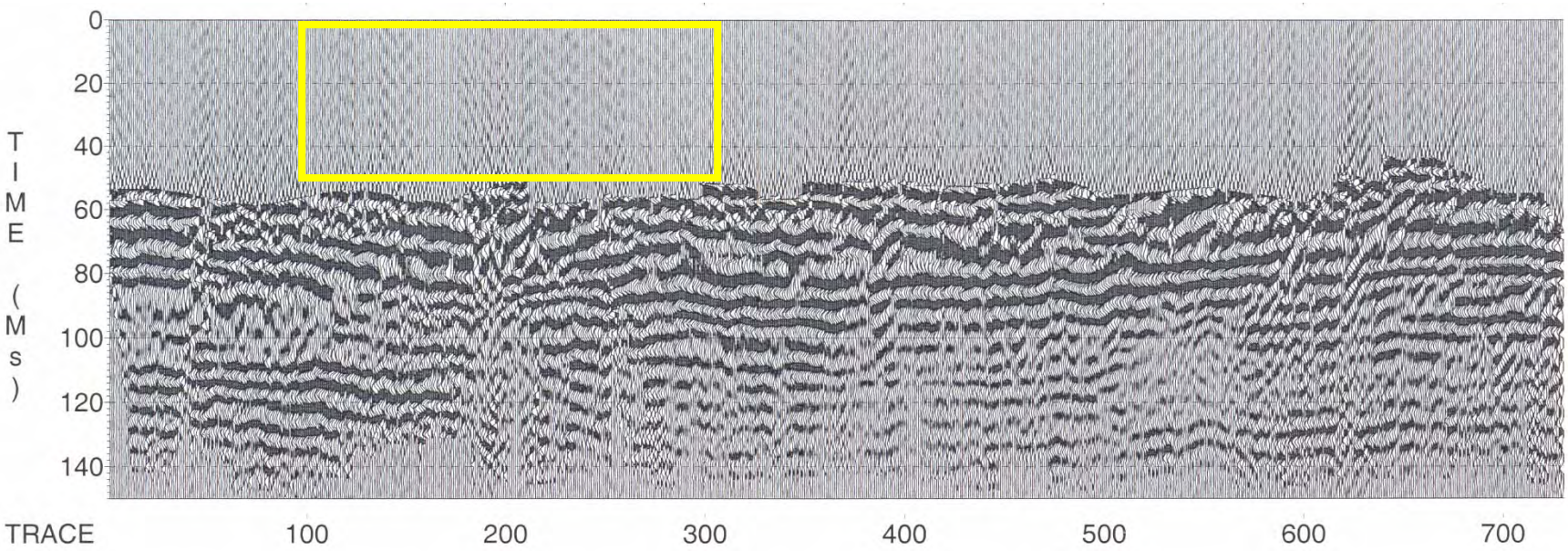

Figure 4.1 Caborn P-wave profile: Acquisition parameters are shown in Table 3.1. The yellow box shows the location of the coincident SH-wave profile (C2).

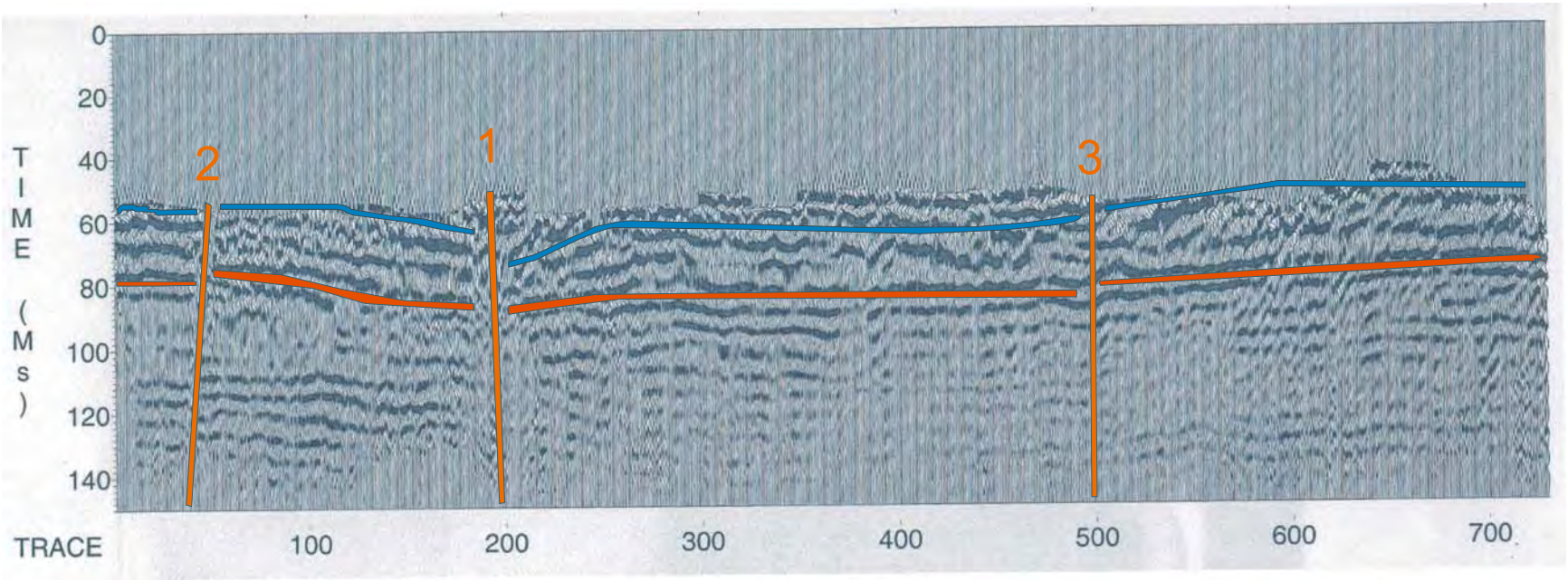

Figure 4.2 Interpretation of Caborn P-wave profile: Blue lines represent the soil/bedrock interface. Red lines represent the most coherent reflector below bedrock. Orange lines and numbers designate faults.

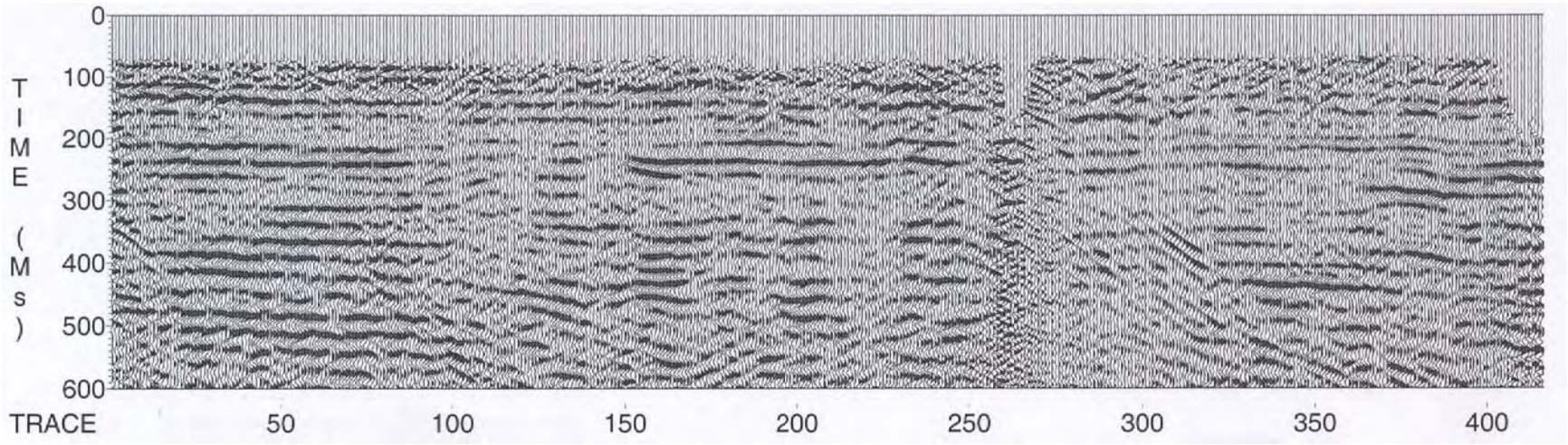

Figure 4.3 Caborn SH-wave profile: Acquisition parameters are shown in Table 3.1. The missing data early in the section between traces 255 and 265 results from a bridge over a small stream.

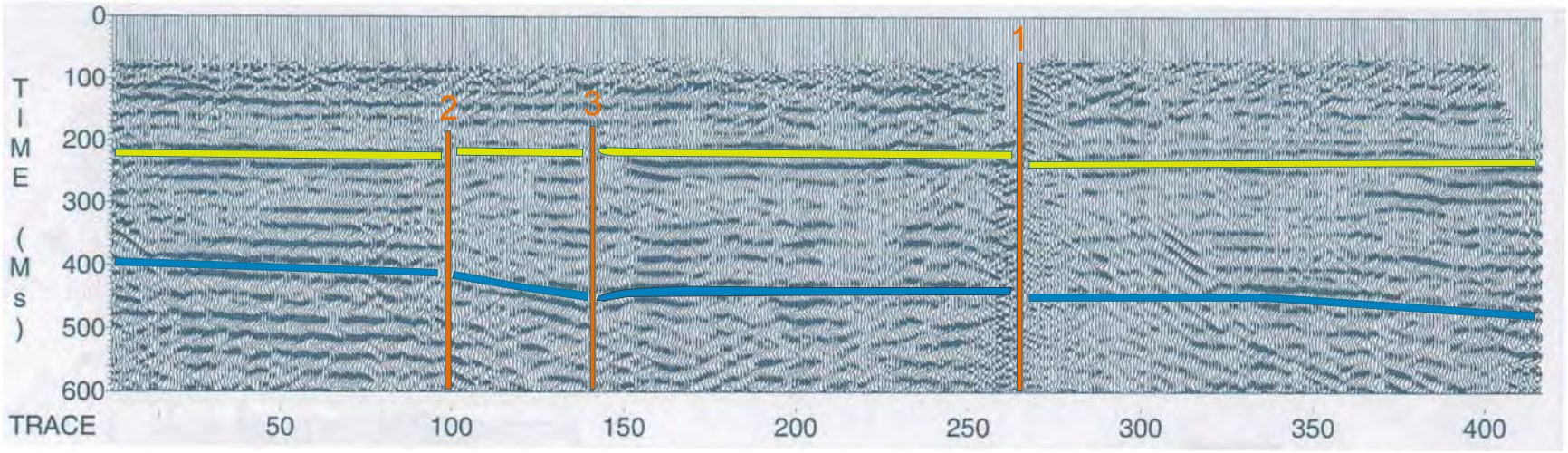

Figure 4.4 Interpretation of Caborn SH-wave profile: Blue lines represent the soil/bedrock interface. Yellow lines represent a soil reflector. Orange lines and numbers designate faults.

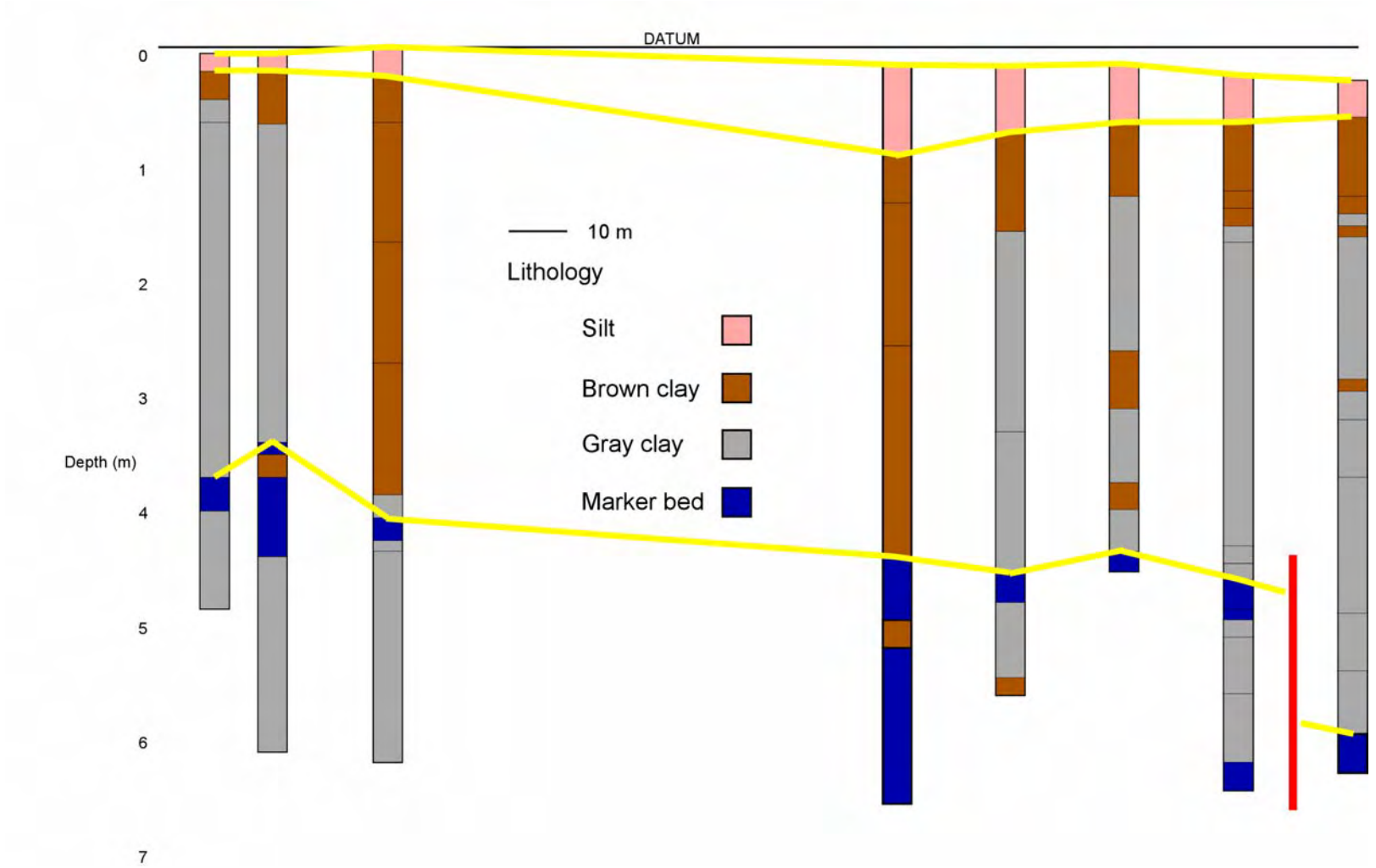

Figure 4.5 Interpretation of Caborn coring: Yellow lines seperate units of like characteristics. Red line represents an interpreted fault.

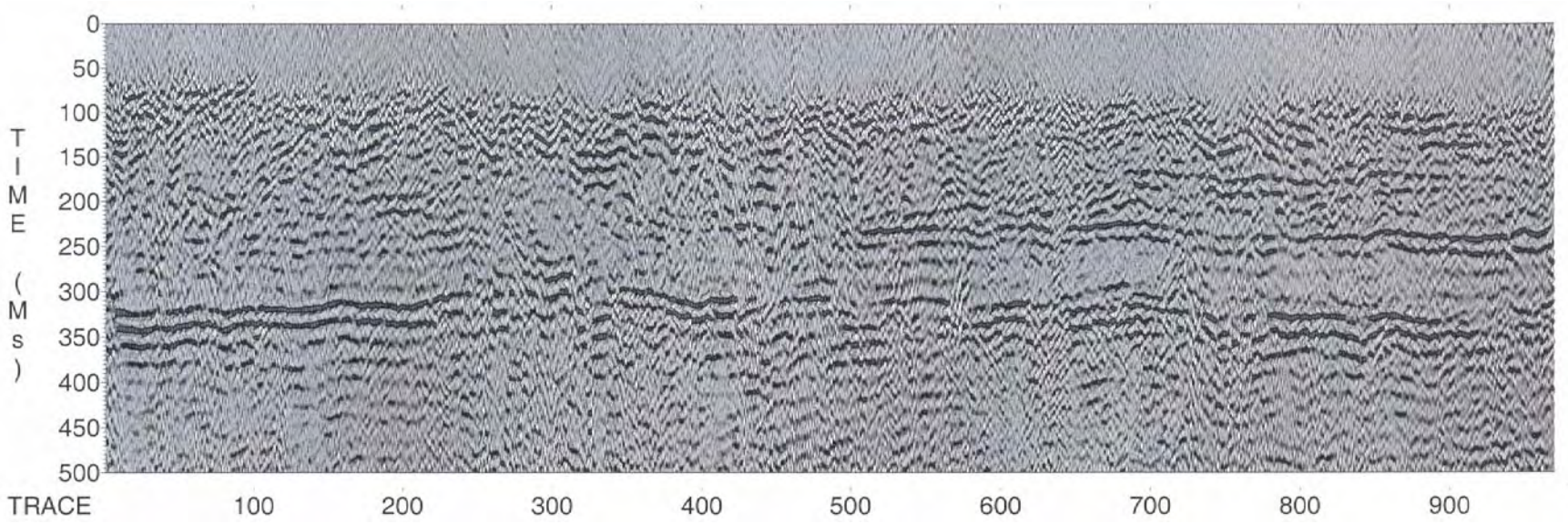

Figure 4.6 Hovey Lake SH-wave profile: Acquisition parameters are shown in Table 3.1.

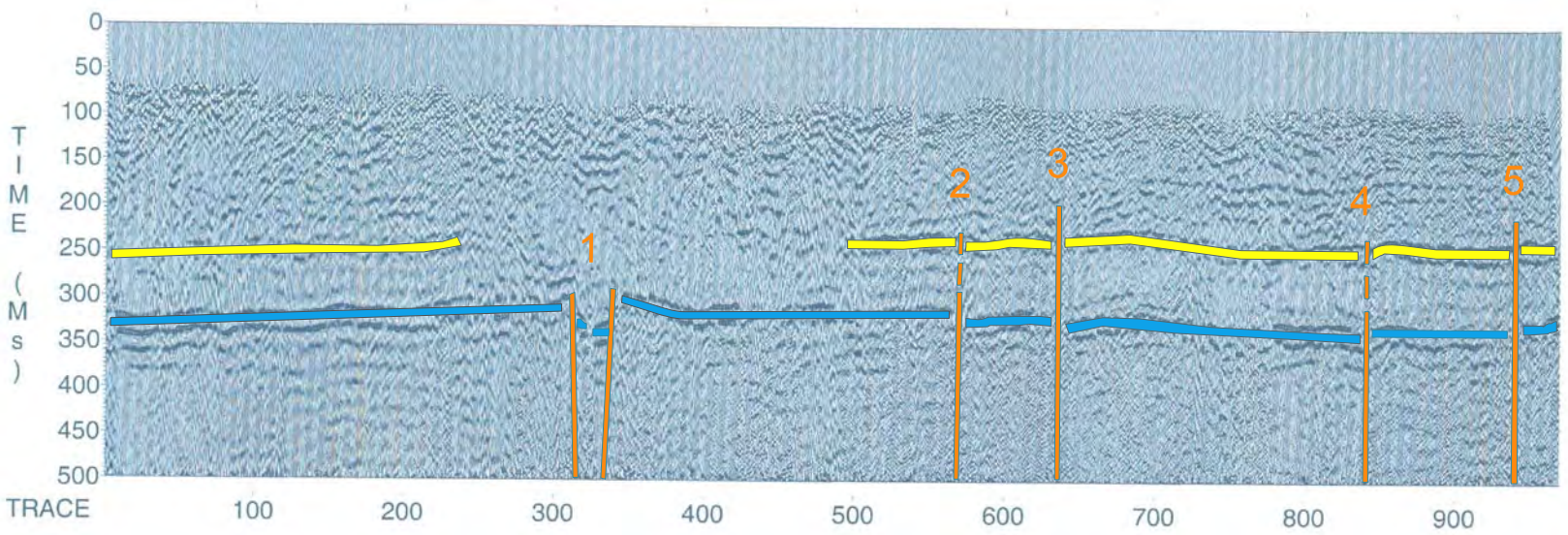

Figure 4.7 Interpretation of Hovey Lake SH-wave profile: Blue lines represent the soil/bedrock interface. Yellow lines represent a soil reflector. Orange lines and numbers designate faults.

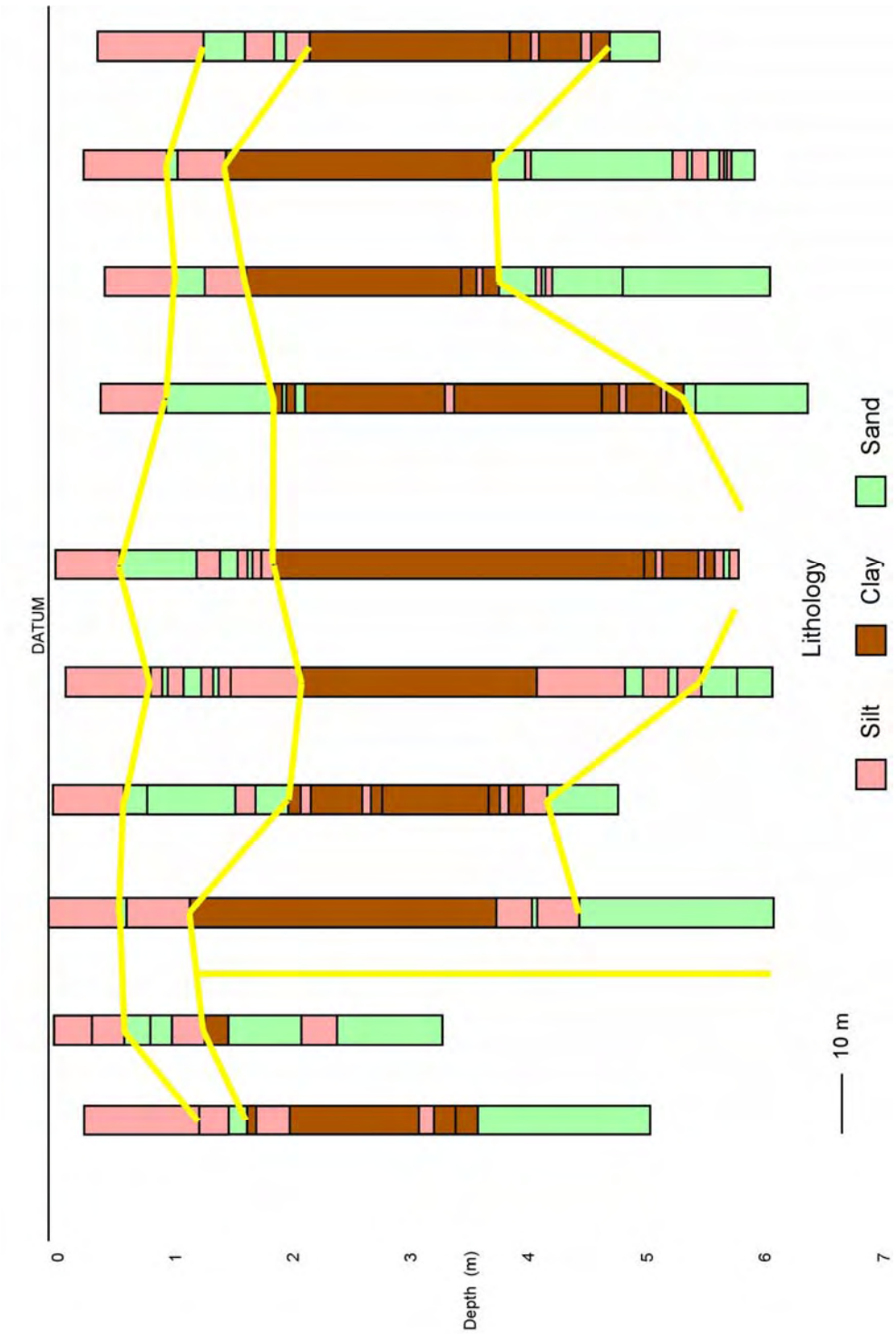

Figure 4.8 Interpretation of Hovey Lake coring: Yellow lines seperate units of like characteristics. Vertical yellow line represents an interpreted channel margin.

5 Conclusions

A one kilometer P-wave seismic-reflection profile, approximately two and a half kilometers of SH-wave seismic-reflection profiles, and twenty-nine correlative boreholes collected in the southern WVFS suggest first-order neotectonic deformation in the Quaternary sediments overlying the reactivated Paleozoic structure. All twelve of the interpreted faults displace soil horizons above high-angle bedrock faults, which support the hypothesis that they are tectonic in origin rather than a result of a surficial process (e.g., slumps, lateral spreading, collapse features, facies change, etc.). The interpreted CF and HLF have displacements at the soil-bedrock interface of approximately 4 and 2.5 m, respectively. The other faults have less significant soil-bedrock displacements of 0.5 to 2 m. Most faults show less displacement along the overlying soil reflectors than at the soil-bedrock interface.

Several styles of deformation were interpreted in the Quaternary overburden: (1) apparent extension, (2) compressional features, such as antiformal folding of layers in the hanging and footwalls, (3) opposing senses of motion with individual faults, and (4) varying slip magnitude within individual faults. Varying types of slip and magnitude of slip along single faults may suggest an oblique component to the fault motion that produces and out-of-plane effect distorting the true slip direction and magnitude in a two-dimensional survey. A dipping layer or layers with varying thickness that are offset obliquely (or laterally) produce a false sense of motion in two dimensions.

The seismic profiles exhibit soil and bedrock layers folded or uplifted by components of compressional stress, rather than reverse-motion slip along high-angle faults. Furthermore, geologically recent fault motions are interpreted to be primarily strike-slip. Apparent normal displacements observed in the Quaternary sediment can result from localized areas of tension (or transtension) that occur in a transpressional fault zone, out-of-plane effects, tensile stresses resulting from compressional uplift of the bedrock and soil, or from actual normal faulting.

The CF and HLF are interpreted to continue into the uppermost 5 m of sediment. Carbon-14 dating of displaced horizons, at the Caborn site, indicates movement after 19,740 YBP. A paleoseismic trenching program is required to determine if the horizon dated at 540 YBP is displaced. These structures represent late Quaternary coseismic deformation, and are considered "capable" structures by the U.S. Army Corps of Engineers and Nuclear Regulatory Commission. The style and timing of deformation within the WVFS, the close association of soil faults to documented Pennsylvania bedrock faults (Hovey Lake fault and Caborn fault), and focal mechanisms in the Wabash Valley seismic zone are all evidence that the extensionally formed Paleozoic faults of the WVFS have been reactivated in the Late Quaternary.

APPENDIX A

Age dating documentation:

BETA

BETA ANALYTIC INC.

DR. M.A. TAMERS and MR. D.G. HOOD

UNIVERSITY BRANCH
4985 S.W. 74 COURT
MIAMI, FLORIDA, USA 33155
PH: 305/667-5167 FAX: 305/663-0964
E-MAIL: beta@radiocarbon.com

REPORT OF RADIOCARBON DATING ANALYSES

Dr. James Whitt

Report Date: 9/19/2006

University of Kentucky

Material Received: 8/16/2006

Sample Data	Measured Radiocarbon Age	13C/12C Ratio	Conventional Radiocarbon Age(*)
Beta - 219989 SAMPLE : SITE2 CORE4 1.13M ANALYSIS : AMS-Standard delivery MATERIAL/PRETREATMENT : (charred material): acid/alkali/acid 2 SIGMA CALIBRATION : Cal AD 1300 to 1440 (Cal BP 640 to 510)	560 +/- 50 BP	-26.3 o/oo	540 +/- 50 BP
Beta - 219990 SAMPLE : SITE 2 CORE4 4.53M ANALYSIS : AMS-Standard delivery MATERIAL/PRETREATMENT : (shell): acid etch	19450 +/- 110 BP	-7.3 o/oo	19740 +/- 110 BP

Dates are reported as RCYBP (radiocarbon years before present, "present" = 1950A.D.). By International convention, the modern reference standard was 95% of the C14 content of the National Bureau of Standards' Oxalic Acid & calculated using the Libby C14 half life (5568 years). Quoted errors represent 1 standard deviation statistics (68% probability) & are based on combined measurements of the sample, background, and modern reference standards.

Measured C13/C12 ratios were calculated relative to the PDB-1 international standard and the RCYBP ages were normalized to -25 per mil. If the ratio and age are accompanied by an (*), then the C13/C12 value was estimated, based on values typical of the material type. The quoted results are NOT calibrated to calendar years. Calibration to calendar years should be calculated using the Conventional C14 age.

CALIBRATION OF RADIOCARBON AGE TO CALENDAR YEARS

(Variables: C13/C12=-26.3:lab. mult=1)

Laboratory number: **Beta-219989**

Conventional radiocarbon age: **540±50 BP**

2 Sigma calibrated result: (95% probability) **Cal AD 1300 to 1440 (Cal BP 640 to 510)**

Intercept data

Intercept of radiocarbon age with calibration curve: Cal AD 1410 (Cal BP 540)

1 Sigma calibrated result: (68% probability) Cal AD 1400 to 1430 (Cal BP 550 to 520)

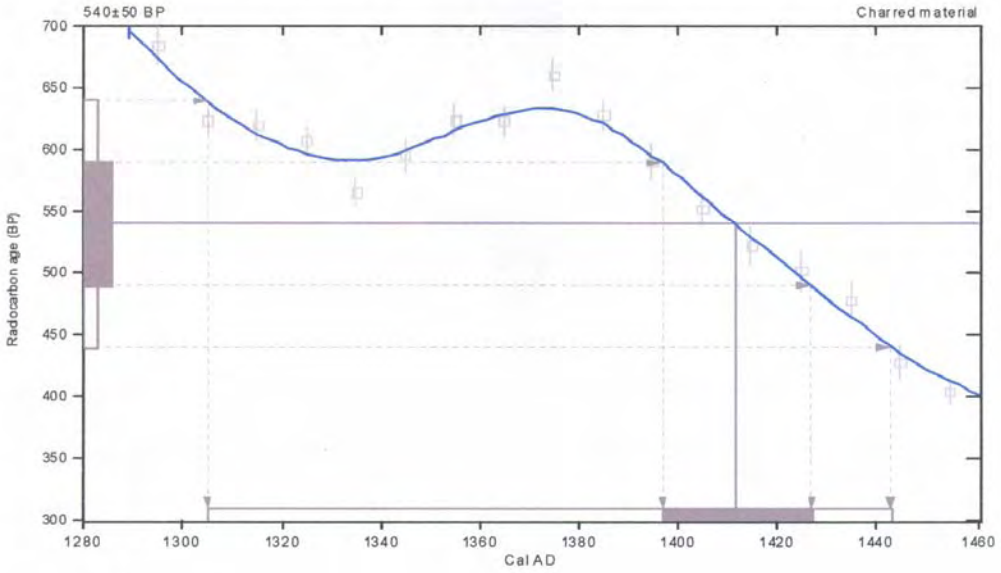

References:

Database used
INTCAL98

Calibration Database

Editorial Comment
Stuiver, M., van der Plicht, H., 1998, Radiocarbon 40(3), pxii-xiii

INTCAL98 Radiocarbon Age Calibration
Stuiver, M., et. al., 1998, Radiocarbon 40(3), p1041-1083

Mathematics

A Simplified Approach to Calibrating C14 Dates
Talma, A. S., Vogel, J. C., 1993, Radiocarbon 35(2), p317-322

Beta Analytic Radiocarbon Dating Laboratory

4985 S.W. 74th Court, Miami, Florida 33155 • Tel: (305)667-5167 • Fax: (305)663-0964 • E-Mail: beta@radiocarbon.com

BETA ANALYYTIC INC. - 4985 SW 74 Court, Miami, Florida 33155 USA - Tel: 305-667-5167 - Fax 305-663-0964 - beta@radiocarbon.com

PRETREATMENT GLOSSARY
Standard Pretreatment Protocols at Beta Analytic

Unless otherwise requested by a submitter or discussed in a final date report, the following procedures apply to pretreatment of samples submitted for analysis. This glossary defines the pretreatment methods applied to each result listed on the date report form (e.g. you will see the designation "acid/alkali/acid" listed along with the result for a charcoal sample receiving such pretreatment).

Pretreatment of submitted materials is required to eliminate secondary carbon components. These components, if not eliminated, could result in a radiocarbon date, which is too young or too old. Pretreatment does not ensure that the radiocarbon date will represent the time event of interest. This is determined by the sample integrity. Effects such as the old wood effect, burned intrusive roots, bioturbation, secondary deposition, secondary biogenic activity incorporating recent carbon (bacteria) and the analysis of multiple components of differing age are just some examples of potential problems. The pretreatment philosophy is to reduce the sample to a single component, where possible, to minimize the added subjectivity associated with these types of problems. If you suspect your sample requires special pretreatment considerations be sure to tell the laboratory prior to analysis.

"acid/alkali/acid"

The sample was first gently crushed/dispersed in deionized water. It was then given hot HCI acid washes to eliminate carbonates and alkali washes (NaOH) to remove secondary organic acids. The alkali washes were followed by a final acid rinse to neutralize the solution prior to drying. Chemical concentrations, temperatures, exposure times, and number of repetitions, were applied accordingly with the uniqueness of the sample. Each chemical solution was neutralized prior to application of the next. During these serial rinses, mechanical contaminants such as associated sediments and rootlets were eliminated. This type of pretreatment is considered a "full pretreatment". On occasion the report will list the pretreatment as "acid/alkali/acid - insolubles" to specify which fraction of the sample was analyzed. This is done on occasion with sediments (See "acid/alkali/acid - solubles"

Typically applied to: charcoal, wood, some peats, some sediments, and textiles "acid/alkali/acid - solubles"

On occasion the alkali soluble fraction will be analyzed. This is a special case where soil conditions imply
That the soluble fraction will provide a more accurate date. It is also used on some occasions to verify the present/absence or degree of contamination present from secondary organic acids. The sample was first pretreated with acid to remove any carbonates and to weaken organic bonds. After the alkali washes (as discussed above) are used, the solution containing the alkali soluble fraction is isolated/filtered and combined with acid. The soluble fraction, which precipitates, is rinsed and dried prior to combustion.

"acid/alkali/acid/cellulose extraction"

Following full acid/alkali/acid pretreatments, the sample is bathed in (sodium chlorite) $NaClO_2$ under very controlled conditions (Ph = 3, temperature = 70 degrees C). This eliminates all components except wood cellulose. It is useful for woods that are either very old or highly contaminated.

Applied to: wood

"acid washes"

Surface area was increased as much a possible. Solid chunks were crushed, fibrous materials were shredded, and sediments were dispersed. Acid (HCI) was applied repeatedly to ensure the absence of carbonates. Chemical concentrations, temperatures, exposure times, and number of repetitions, were applied accordingly with the uniqueness of each sample. The sample was not be subjected to alkali washes to ensure the absence of secondary organic acids for intentional reasons. The most common reason is that the primary carbon is soluble in the alkali. Dating results reflect the total organic content of the analyzed material. Their accuracy depends on the researcher's ability to subjectively eliminate potential contaminants based on contextual facts.

Typically applied to: organic sediments, some peats, small wood or charcoal, special cases

BETA ANALYYTIC INC. - 4985 SW 74 Court, Miami, Florida 33155 USA - Tel: 305-667-5167 - Fax 305-663-0964 - beta@radiocarbon.com

PRETREATMENT GLOSSARY
Standard Pretreatment Protocols at Beta Analytic
(Continued)

"collagen extraction: with alkali or collagen extraction: without alkali

The material was first tested for friability ("softness"). Very soft bone material is an indication of the potential absence of the collagen fraction (basal bone protein acting as a "reinforcing agent" within the crystalline apatite structure). It was then washed in de-ionized water, the surface scraped free of the outer most layers and then gently crushed. Dilute, cold HCI acid was repeatedly applied and replenished until the mineral fraction (bone apatite) was eliminated. The collagen was then dissected and inspected for rootlets. Any rootlets present were also removed when replenishing the acid solutions. "With alkali" refers to additional pretreatment with sodium hydroxide (NaOH) to ensure the absence of secondary organic acids. "Without alkali" refers to the NaOH step being skipped due to poor preservation conditions, which could result in removal of all available organics if performed.

Typically applied to: bones

"acid etch"

The calcareous material was first washed in de-ionized water, removing associated organic sediments and debris (where present). The material was then crushed/dispersed and repeatedly subjected to HCI etches to eliminate secondary carbonate components. In the case of thick shells, the surfaces were physically abraded prior to etching down to a hard, primary core remained. In the case of porous carbonate nodules and caliches, very long exposure times were applied to allow infiltration of the acid. Acid exposure times, concentrations, and number of repetitions, were applied accordingly with the uniqueness of the sample.

Typically applied to: shells, caliches, and calcareous nodules

"neutralized"

Carbonates precipitated from ground water are usually submitted in an alkaline condition (ammonium Hydroxide or sodium hydroxide solution). Typically this solution is neutralized in the original sample container, using deionized water. If larger volume dilution was required, the precipitate and solution were transferred to a sealed separatory flask and rinsed to neutrality. Exposure to atmosphere was minimal.

Typically applied to: Strontium carbonate, Barium carbonate
(i.e. precipitated ground water samples)

"carbonate precipitation"

Dissolved carbon dioxide and carbonate species are precipitated from submitted water by complexing them as ammonium carbonate. Strontium chloride is added to the ammonium carbonate solution and strontium carbonate is precipitated for the analysis. The result is representative of the dissolved inorganic carbon within the water. Results are reported as "water DIC".

Applied to: water

"solvent extraction"

The sample was subjected to a series of solvent baths typically consisting of benzene, toluene, hexane, pentane, and/or acetone. This is usually performed prior to acid/alkali/acid pretreatments.

Applied to: textiles, prevalent or suspected cases of pitch/tar contamination, conserved materials.

"none"

No laboratory pretreatments were applied. Special requests and pre-laboratory pretreatment usually accounts for this.

BETA

Consistent Accuracy ...
Delivered On Time.

Beta Analytic Inc.
4985 SW 74 Court
Miami, Florida 33155 USA
Tel: 305 667 5167
Fax: 305 663 0/97
Beta@radiocarbon.com
Www.radiocarbon.com

Mr. Darden Hood
Director

Mr. Ronald Hatfield
Mr. Christopher Patrick
Deputy Directors

Final Report

The final report package includes the final date report, a statement outlining our analytical procedures, a glossary of pretreatment terms, calendar calibration information, billing documents (containing balance/credit information and the number of samples submitted within the yearly discount period), and peripheral items to use with future submittals. The final report includes the individual analysis method, the delivery basis, the material type and the individual pretreatments applied. The final report has been sent by mail and e-mail (where available).

Pretreatment

Pretreatment methods are reported along with each result. All necessary chemical and mechanical pretreatments of the submitted material were applied at the laboratory to isolate the carbon which may best represent the time event of interest. When interpreting the results, it is important to consider the pretreatments. Some samples cannot be fully pretreated, making their ^{14}C ages more subjective than samples which can be fully pretreated. Some materials receive no pretreatments. Please look at the pretreatment indicated for each sample and read the pretreatment glossary to understand the implications.

Analysis

Materials measured by the radiometric technique were analyzed by synthesizing sample carbon to benzene (92% C), measuring for ^{14}C content in one of 53 scintillation spectrometers, and then calculating for radiocarbon age. If the Extended Counting Service was used, the ^{14}C content was measured for a greatly extended period of time. AMS results were derived from reduction of sample carbon to graphite (100% C), along with standards and backgrounds. The graphite was then detected for ^{14}C content in one of 9 accelerator-mass-spectrometers (AMS) .

The Radiocarbon Age and Calendar Calibration

The "Conventional ^{14}C Age (*)" is the result after applying $^{13}C/^{12}C$ corrections to the measured age and is the most appropriate radiocarbon age. If an "*" is attached to this date, it means the $^{13}C/^{12}C$ was estimated rather than measured (The ratio is an option for radiometric analysis, but included on all AMS analyses.) Ages are reported with the units "BP" (Before Present). "Present" is defined as AD 1950 for the purposes of radiocarbon dating.

Results for samples containing more ^{14}C than the modern reference standard are reported as "percent modern carbon" (pMC). These results indicate the material was respiring carbon after the advent of thermo-nuclear weapons testing (and is less than ~ 50 years old).

Applicable calendar calibrations are included for materials between about 100 and 19,000 BP. If calibrations are not included with a report, those results were either too young, too old, or inappropriate for calibration. Please read the enclosed page discussing calibration.

BETA

Consistent Accuracy ...
Delivered On Time.

Beta Analytic Inc.
4985 SW 74 Court
Miami, Florida 33155 USA
Tel: 305 667 5167
Fax: 305 663 0/97
Beta@radiocarbon.com
Www.radiocarbon.com

Mr. Darden Hood
Director

Mr. Ronald Hatfield
Mr. Christopher Patrick
Deputy Directors

Calendar Calibration at Beta Analytic

Calibrations of radiocarbon age determinations are applied to convert BP results to calendar years. The short-term difference between the two is caused by fluctuations in the heliomagnetic modulation of the galactic cosmic radiation and, recently, large scale burning of fossil fuels and nuclear devices testing. Geomagnetic variations are the probable cause of longer-term differences.

The parameters used for the corrections have been obtained through precise analyses of hundreds of samples taken from known-age tree rings of oak, sequoia, and fir up to about 10,000 BP. Calibration using tree-rings to about 12,000 BP is still being researched and provides somewhat less precise correlation. Beyond that, up to about 20,000 BP, correlation using a modeled curve determined from U/Th measurements on corals is used. This data is still highly subjective. Calibrations are provided up to about 19,000 years BP using the most recent calibration data available.

The Pretoria Calibration Procedure (Radiocarbon, Vol 35, No.1, 1993, pg 317) program has been chosen for these calendar calibrations. It uses splines through the tree-ring data as calibration curves, which eliminates a large part of the statistical scatter of the actual data points. The spline calibration allows adjustment of the average curve by a quantified closeness-of-fit parameter to the measured data points. A single spline is used for the precise correlation data available back to 9900 BP for terrestrial samples and about 6900 BP for marine samples. Beyond that, splines are taken on the error limits of the correlation curve to account for the lack of precision in the data points.

In describing our calibration curves, the solid bars represent one sigma statistics (68% probability) and the hollow bars represent two sigma statistics (95% probability). Marine carbonate samples that have been corrected for $^{13}C/^{12}C$, have also been corrected for both global and local geographic reservoir effects (as published in Radiocarbon, Volume 35, Number 1, 1993) prior to the calibration. Marine carbonates that have not been corrected for $^{13}C/^{12}C$ are adjusted by an assumed value of 0 %0 in addition to the reservoir corrections. Reservoir corrections for fresh water carbonates are usually unknown and are generally not accounted for in those calibrations. In the absence of measured $^{13}C/^{12}C$ ratios, a typical value of -5 %0 is assumed for freshwater carbonates.

(Caveat: the correlation curve for organic materials assume that the material dated was living for exactly ten years (e.g. a collection of 10 individual tree rings taken from the outer portion of a tree that was cut down to produce the sample in the feature dated). For other materials, the maximum and minimum calibrated age ranges given by the computer program are uncertain. The possibility of an "old wood effect" must also be considered, as well as the potential inclusion of younger or older material in matrix samples. Since these factors are indeterminant error in most cases, these calendar calibration results should be used only for illustrative purposes. In the case of carbonates, reservoir correction is theoretical and the local variations are real, highly variable and dependent on provenience. Since imprecision in the correlation data beyond 10,000 years is high, calibrations in this range are likely to change in the future with refinement in the correlation curve. The age ranges and especially the intercept ages generated by the program must be considered as approximations.)

CALIBRATION OF RADIOCARBON AGE TO CALENDAR YEARS

Variables used in the calculation of age calibration → (Variables: est. C13/C12=-25:lab. mult=1)

Laboratory number: **Beta-123456**

The uncalibrated Conventional Radiocarbon Age (± 1 sigma)

Conventional radiocarbon age[1]: **2400±60 BP**

The calendar age range in both calendar years (AD or BC) and in Radiocarbon Years (BP)

2 Sigma calibrated result: (95% probability) **Cal BC 770 to 380 (Cal BP 2720 to 2330)**

[1] *C13/C12 ratio estimated*

Intercept data

The intercept between the average radiocarbon age and the calibrated curve time scale. This value is illustrative and should not be used by itself.

Intercept of radiocarbon age with calibration curve: Cal BC 410 (Cal BP 2360)

1 Sigma calibrated result: (68% probability) Cal BC 740 to 710 (Cal BP 2690 to 2660) and Cal BC 535 to 395 (Cal BP 2485 to 2345)

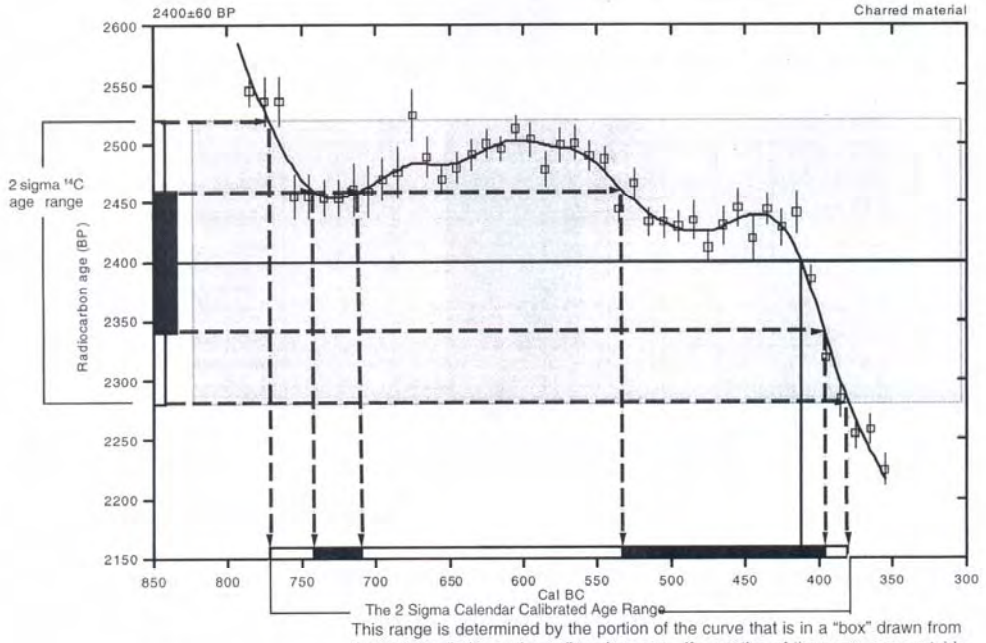

This range is determined by the portion of the curve that is in a "box" drawn from the 2 sigma limits on the radiocarbon age. If a section of the curve goes outside of the "box", multiple ranges will occur as shown by the two 1 sigma ranges which occur from sections going outside of a similar "box" which would be drawn at the 1 sigma limits.

References:

Database used
Intcal 98
Calibration Database
Editorial Comment
Stuiver, M., van der Plicht, H., 1998, Radiocarbon 40(3), pxii-xiii
INTCAL98 Radiocarbon Age Calibration
Stuiver, M., et. al., 1998, Radiocarbon 40(3), p1041-1083
Mathematics
A Simplified Approach to Calibrating C14 Dates
Talma, A. S., Vogel, J. C., 1993, Radiocarbon 35(2), p317-322

References for the calibration data and the mathematics applied to the data. These references, as well as the Conventional Radiocarbon Age and the 13C/12C ratio used should be included in your papers.

Beta Analytic Radiocarbon Dating Laboratory

4985 S.W. 74th Court, Miami, Florida 33155 • Tel: (305)667-5167 • Fax: (305)663-0964 • E-mail: beta@radiocarbon.com

Appendix B

Second part of line C1:

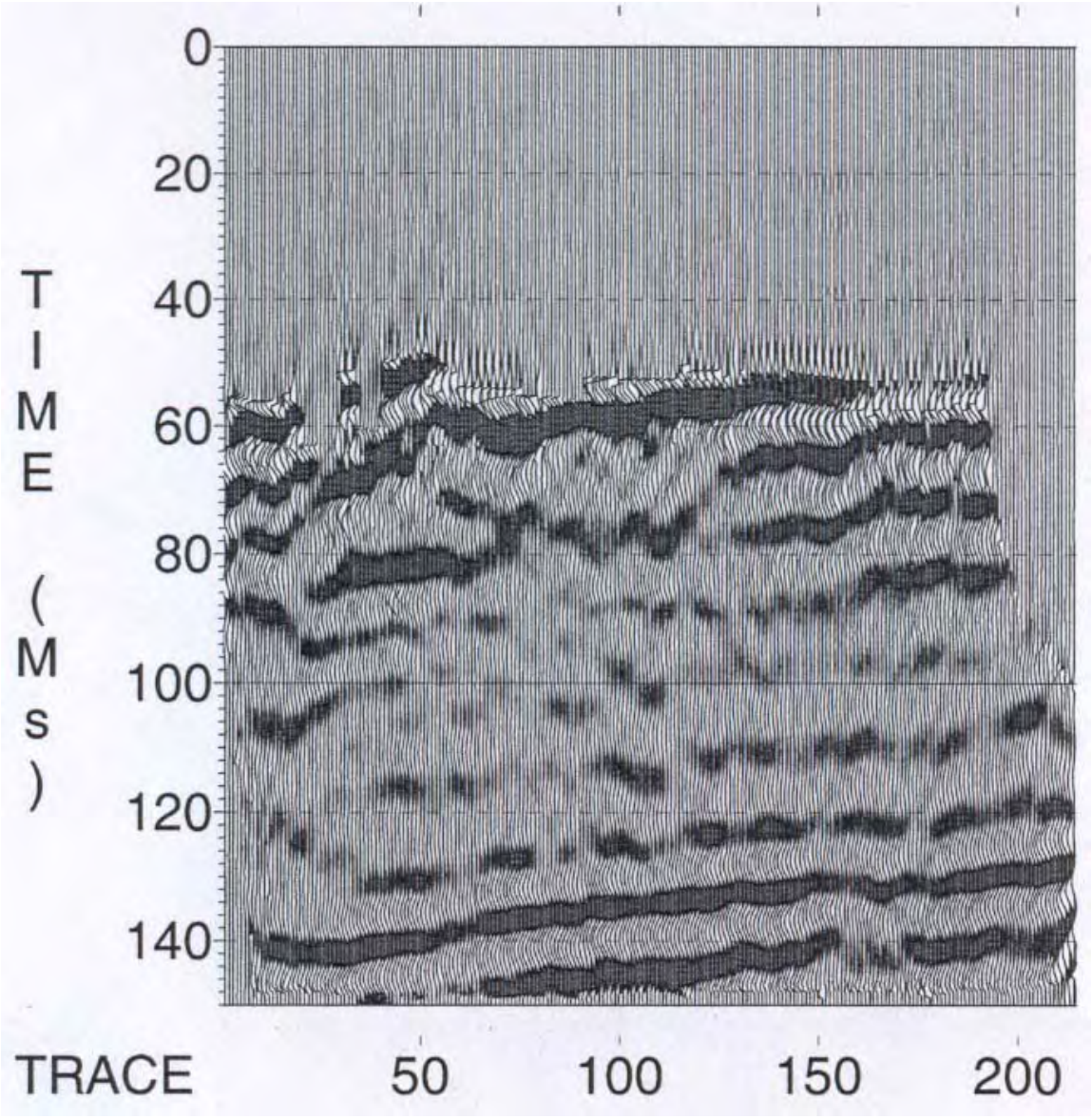

BIBLIOGRAPHY

Baker, G.S., 1999, Processing near-surface seismic-reflection data – A primer: Soc. of Explor. Geophy., Course Notes Series No. 9, Roger Young ed., 77p.

Bear, G.W., Rupp, J.A., and Rudman, A.J., 1997, Seismic interpretation of the deep structure of the Wabash Valley Fault System: Seismological Research Letters, v. 68, no. 4, p. 624-640.

Braile, L.W., Keller, G.R., Hinze, W.J., Lidiak, E.G., 1982, An ancient rift complex and its relation to contemporary seismicity in the New Madrid seismic zone: Tectonics, v. 1, p. 225-237.

Braile, L.W., Hinze, W.J., Keller, G.R., Lidiak, E.G., and Sexton, J.L., 1986, Tectonic development of the New Madrid rift complex, Mississippi Embayment, North America: Tectonophysics, v. 131, no. 1-2, p. 1-21.

Braile, L.W., Hinze, W.J., and Keller, G.R., 1997, New Madrid seismicity, gravity anomalies, and interpreted ancient rift structures: Seismological Research Letters, v. 68, no. 4, p. 599-610.

Bristol, H.M., and Treworgy, J.D., 1979, The Wabash Valley Fault System in southeastern Illinois: Illinois State Geological Survey, Circular 509.

FMSM Engineers, 2002, Final Report – J.T. Meyers Locks and Dam Seismological Study.

Harris, J.B., 1996, Shear-wave splitting in Quaternary sediments: Neotectonic implications in the central New Madrid seismic zone: Geophysics, v. 61, no. 6 (November-December 1996), p. 1871-1882.

Heigold, P.C. and Kolata, D.R., 1993, Proterozoic crustal boundary in the southern part of the Illinois Basin: Tectonophysics, v. 217, p. 307-319.

Hildenbrand, T.G., 1985, Rift structure of the northern Mississippi Embayment from the analysis of gravity and magnetic data: Journal of Geophysical Research, v. 90, no. B14, p. 12,607-12,622.

Hildenbrand, T.G., Kucks, R.P., and Heigold, P.C., 1996, Magnetic and gravity study of the Paducah 1º X 2º CUSMAP Quadrangle, Illinois, Indiana, Kentucky, and Missouri: U.S. Geological Survey Bulletin 2150-C, 22 p.

Johnson, W.D., and Norris, R.L., 1976, Geologic map of parts of the Uniontown and Wabash Island quadrangles, Union and Henderson Counties, Kentucky, U.S. Geol. Surv. Geological Quadrangle Map GQ-1291.

Kim, W-Y, 2003, The 18June2002 Caborn, Indiana, Earthquake: Reactivation of Ancient Rift in the Wabash Valley Seismic Zone: Bulletin of the Seismological Society of America, v. 93, p. 2201-2211.

Kim, W-Y, 2006, Personal Communication, 78th Annual Meeting of the Eastern Section of the Seismological Society of America Meeting, October 2-4, 2006, Ottawa, Ca.

Kolata, D.R., and Hildenbrand, T.G., 1997, Structural underpinnings and neotectonics of the southern Illinois basin: an overview, Seismological Research Letters, v. 68, p. 499-510.

Kolata, D.R., and Nelson, W.J., 1991, Tectonic History of the Illinois Basin: Am. Assoc. Pet. Geol., Mem. 51.

McBride, J.H., M.L. Sargent, and C.J. Potter (1997). Investigating possible earthquake-related structure beneath the southern Illinois Basin from seismic reflection, Seismological Research Letters, v. 68, p. 641-649.

McBride, J., Nelson, J., and W.J. Stephenson, 2002, Integrated geological and geophysical study of Quaternary-age deformation in the northern Mississippi embayment: Seismological Research Letters, v. 73, p. 597-627.

McBride, J., Pugin, A., Nelson, W., Larson, T., Sargent, S., Devera, J., Denny, F., and Woolery, E., 2003, Unusual and variable post-Paleozoic deformation detected by seismic reflection profiling across northwestern "prong" of New Madrid seismic zone, Tectonophysics, v. 368, p. 171-191.

Munson, P.J., C.A. Munson, and E.C. Pond, 1995, Paleoliquefaction evidence for strong earthquake shaking in south-central Indiana, Geology, v. 23, 325-328.

Munson, P.J., S.F. Obermeier, C.A. Munson, and E.R. Hajic (1997). Liquefaction evidence for Holocene and latest Pleistocene seismicity in the southern halves of Indiana and Illinois: A preliminary overview, Seismological Research Letters, v. 68, 521-536.

Obermeier, S.F., J. R. Martin, A.D. Frankel, T.L. Youd, P.J. Munson, C.A. Munson, and E.C. Pond (1993). Liquefaction evidence for one or more strong Holocene earthquakes in the Wabash Valley of southern Indiana and Illinois, with a preliminary estimate of magnitude, U.S. Geol. Surv. Prof. Paper 1536, 26 p.

Pond, E.C. and Martin, J.R., 1997, Estimated magnitudes and accelerations associated with prehistoric earthquakes in the Wabash Valley region of the central United States: Seismological Research Letters, v. 68, no. 4, p. 611-623.

Rene, R.M. and Stanonis, F.L., 1995, Reflection seismic profiling of the Wabash Valley fault system in the Illinois Basin: USGS Professional Paper 1538-O.

Rutledge III, F. A., 2004, High-resolution Geophysical Investigation of Late Quaternary Deformation in the Lower Wabash Valley Fault System, Master's Thesis, University of Kentucky.

Schweig III, E.S., Shen, F., Kanter, L.R., Luzietti, E.A., VanArsdale, R.B., Shedlock, K.M., and King, K.W., Shallow Seismic Reflection Survey of the Bootheel Lineament Area, Southeastern Missouri: Seismological Research Letters, v. 63, no.3, July-September, 1992, p. 285-295.

Smith, D.G. and Jol, H.M., 1995, Ground penetrating radar – Antenna frequencies and maximum probable depths of penetration in Quaternary sediments: Applied Geophysics, v. 33, p. 93-100.

Stein, S. and Wysession, M., 2003, An Introduction to Seismology, Earthquakes, and Earth Structure, Blackwell Publishing, p.141-144.

Taylor, K.B., Herrman, R.B., Hamburger, M.W., Pavlis, G.L., Johnston, A., Lager, C., and Lam, C., 1989, The southestern Illinois earthquake of 10 June 1987: Seismological Research Letters, v. 60, no. 3, p. 101-109.

Wheeler, R.L., 1997, Boundary separating the seismically active Reelfoot Rift from the sparsely seismic Rough Creek Graben, Kentucky and Illinois: Seismological Research Letters, v. 68, no. 4, p. 586-598.

Woolery, E. W., Street, R., Wang, Z., and Harris, J., 1993, Near-surface deformation in the New Madrid seismic zone as imaged by high-resolution SH-wave seismic methods: Geophysical Research Letters, v. 20, p. 1615-1618.

Woolery, E. W., Wang, Z., Street, R. L., and Harris, J. B., 1996, A P- and SH-wave seismic investigation of the Kentucky Bend fault scarp in the New Madrid seismic zone: Seismological Research Letters, v. 66, p. 67-74.

Woolery, E. W. and Street, R., 2002, Quaternary fault reactivation in the Fluorspar Area Fault Complex of western Kentucky – Evidence from shallow SH-wave reflection profiles: Seismological Research Letters, v. 73. p. 628-639.

Woolery, E. W., Schaefer, J., and Wang, Z., 2003, Elevated Lateral Stress in Unlithified Sediment, Midcontinent, United States-Geotechnical and Geophysical Indicators for a Tectonic Origin, Tectonophysics, v. 368, p. 139-153.

Woolery, E. W., Rutledge, F. A., and VanArsdale, R. B., 2004, High-resolution Geophysical and Geological Investigations of Late Quaternary Deformation in the Lower Wabash Valley Fault Zone, U.S. Geological Survey- National Earthquake Hazards Reduction Program Final Technical Report: 04HQGR0094, 100 p.

Woolery, E. W., 2005, Geophysical and Geological Evidence of Neotectonic Deformation along the Hovey Lake Fault, Lower Wabash Valley Fault System, Central United States, Bulletin of the Seismological Society of America, Vol. 95, No. 3, pp. 1193-1201.

www.munsell.com

www.soilsample.com